Scalar field critical collapse in 2+1 dimensions

Joanna Jałmużna,[1] Carsten Gundlach,[2] and Tadeusz Chmaj[3, 4]

[1]*Institute of Physics, Jagiellonian University, Kraków, Poland*
[2]*Mathematical Sciences, University of Southampton, Southampton SO17 1BJ, United Kingdom*
[3]*Cracow University of Technology, Kraków, Poland*
[4]*Institute of Nuclear Physics, Polish Academy of Science, Kraków, Poland*

We carry out numerical experiments in the critical collapse of a spherically symmetric massless scalar field in 2+1 spacetime dimensions in the presence of a negative cosmological constant and compare them against a new theoretical model. We approximate the true critical solution as the $n = 4$ Garfinkle solution, matched at the lightcone to a Vaidya-like solution, and corrected to leading order for the effect of $\Lambda < 0$. This approximation is only C^3 at the lightcone and has three growing modes. We *conjecture* that pointwise it is a good approximation to a yet unknown true critical solution that is analytic with only one growing mode (itself approximated by the top mode of our amended Garfinkle solution). With this conjecture, we predict a Ricci-scaling exponent of $\gamma = 8/7$ and a mass-scaling exponent of $\delta = 16/23$, compatible with our numerical experiments.

CONTENTS

I. INTRODUCTION

A. Critical collapse

Starting with Choptuik's investigation of scalar field collapse [1], and since then generalised to many other systems [2], critical collapse is concerned with the threshold of black hole formation in the space of initial data. A practical way of investigating this threshold is to pick any one-parameter family of asymptotically flat initial data, with parameter p, such that for $p > p_*$ the data form a black hole, and for $p < p_*$ they do not.

More specifically, "type II" critical collapse is concerned with the case where the black hole mass can be made arbitrarily small at the threshold. A necessary condition for this to happen is that the system of Einstein equations and matter evolution equations is scale-invariant, or effectively scale-invariant on sufficiently small length scales. As far as we know, exact scale-invariance is also sufficient for the existence of type II critical collapse.

In type II critical collapse in $d + 1$ spacetime dimensions, for $p < p_*$ ("subcritical" data), the maximum value of curvature (say the Ricci scalar) achieved on the spacetime scales as

$$|R|_{\max} \sim (p_* - p)^{-2\gamma} \qquad (1)$$

and for $p > p_*$ ("supercritical" data), the black hole mass scales as

$$M_{BH} \sim (p - p_*)^{\delta} \qquad (2)$$

where in $d \geq 3$

$$\delta = \gamma(d - 2). \qquad (3)$$

The relation (3) follows essentially from dimensional analysis, with $d - 2$ the dimension (in gravitational units

$c = G = 1$) of mass (or energy). The exponent γ depends on the type of matter and spacetime dimension, but is universal for all 1-parameter families of initial data.

In a small spacetime region just before the point of maximum curvature, or just before the formation of an apparent horizon, the spacetime and matter field are approximated by a "critical solution" which is again universal for a given system and spacetime dimension. The critical solution has three defining properties: it is regular, scale-invariant (continuously self-similar, CSS) or scale-periodic (discretely self-similar, DSS), and it has precisely one unstable mode. Continuous self-similarity means that there is a conformal Killing vector field K such that $\mathcal{L}_K g_{ab} = -2g_{ab}$. In coordinates (x, T) adapted to CSS and spherical symmetry (but otherwise general), such that $K = \partial/\partial T$, this means that the metric takes the form

$$ds^2 = \ell^2 e^{-2T}[A(x)\,dT^2 + 2B(x)\,dT\,dx + C(x)\,dx^2$$
$$+R^2(x)\,d\Omega_{d-1}^2], \tag{4}$$

where ℓ is an arbitrary length scale. This functional form of the metric is invariant under gauge transformations of the form

$$x \to F(x), \qquad T \to T + G(x). \tag{5}$$

[In DSS, in adapted coordinates, the metric takes the same form, with A, B, C, R (and F, G) now depending periodically on T with some scale-echoing period Δ.]

The most general ansatz for a massless scalar field that is compatible, via the Einstein equations with $\Lambda = 0$, with continuous self-similarity of the metric is the Christodoulou ansatz [14]

$$\phi(x, T) = cT + f(x) \tag{6}$$

for some constant c. [For DSS, $f = f(x, T)$ depends also on T with period Δ.] The constant c does not depend on the choice of similarity coordinates. The spherical scalar field critical solution in higher dimensions is DSS with $c = 0$ but, as we shall see later, in 2+1 dimensions it seems to be CSS with $c \neq 0$.

In a spherically symmetric critical solution, the regular centre corresponds to one value of x. $T = \infty$ (for all x) represents a single spacetime point at the centre, the accumulation point, where the curvature blows up. Another value of x corresponds to the past lightcone (or soundcone, for fluid matter) of the accumulation point, where the critical solution must also be regular. The critical solution can be continued in x to the future lightcone of the accumulation point. Beyond the future lightcone, there is no unique continuation, but that part of the critical solution is not relevant for critical collapse.

If we choose T to be timelike or null, we can interpret it both as a time coordinate on spacetime and as the logarithm of scale in renormalisation group theory. From self-similarity and the existence of precisely one unstable mode, using a little dynamical systems theory and

dimensional analysis, one can then derive both universality and the above scaling relations. γ turns out to be the inverse Lyapunov exponent of the one unstable mode.

This scaling argument [2, 3] goes roughly as follows: the closer p to p_*, the smaller the initial value of the one growing mode, the longer (larger T) the spacetime stays close to the critical solution. But larger T also means scalar field variation on smaller length scales, and hence larger curvature, before the solution either starts dispersing or forms an apparent horizon.

For a spherically symmetric massless scalar field in the presence of a negative cosmological constant, critical collapse has been investigated in 3+1 dimensions [4]. In higher dimensions, critical collapse has been investigated in [5] for $\Lambda = 0$, and in [6] for $\Lambda < 0$. A cosmological constant (of either sign) obviously breaks scale-invariance, but one would expect it to become negligible in regions of sufficiently large curvature, and hence in the regime where type II critical phenomena are seen. Indeed this seems to be the case in 3+1 and higher dimensions. A further effect of a negative cosmological constant is to replace asymptotic flatness with asymptotically anti-deSitter (adS) boundary conditions. The only boundary conditions for a massless scalar field compatible with the Einstein equations are totally reflecting. As a consequence, it appears that arbitrarily weak generic initial data collapse after sufficiently many reflections off the boundary. (But see [7] for exceptions to this). However, at the thresholds p_{*0}, p_{*1}, p_{*2} for black hole formation after zero, one, two, and so on, reflections the same type II critical phenomena are seen as in asymptotically flat spacetime. Because of the reflecting boundaries, all the mass must fall into the black hole eventually, but the mass of the apparent horizon when it first forms does scale, with the same γ as the black hole mass in asymptotically flat spacetime.

B. 2+1 dimensions

The situation is quite different in 2+1 dimensions. First, this is the critical dimension for the wave equation, meaning that the scalar field energy ($|\nabla\phi|^2$ integrated over d space dimensions) is dimensionless. Similarly, for gravity the black hole mass and the 2+1 dimensional equivalent of the Hawking mass are dimensionless. This already indicates that any mass scaling cannot be derived using the standard dimensional analysis argument. Secondly, in the absence of a cosmological constant there are no black hole solutions, and finite mass regular initial data cannot form an apparent horizon dynamically.

Standard gauge choices in spherical symmetry in $2+1$ spacetime dimensions are polar-radial coordinates $(\bar{r}, \bar{t})$,

$$ds^2 = e^{2\alpha}\left(-e^{2\beta}d\bar{t}^2 + d\bar{r}^2\right) + \bar{r}^2\,d\theta^2, \tag{7}$$

where the area radius $\bar{r}$ is a coordinate, and double null coordinates (u, v),

$$ds^2 = -e^{2\mathcal{A}}du\,dv + \bar{r}^2\,d\theta^2, \tag{8}$$

where $\bar{r}$ is a metric coefficient. With $u =: t - r$ and $v =: t + r$, this can also be written as

$$ds^2 = e^{2\mathcal{A}}(-dt^2 + dr^2) + \bar{r}^2\, d\theta^2. \qquad (9)$$

[In $d + 1$ dimensions, the same coordinate choices exist, with $d\theta^2$ replaced by the line element on the unit $(d-1)$-sphere.]

In 2+1 dimensions, the field equations

$$G_{ab} + \Lambda g_{ab} = \kappa[\nabla_a\phi\nabla_b\phi - \tfrac{1}{2}g_{ab}(\nabla\phi)^2], \quad \nabla^2\phi = 0 \quad (10)$$

for the metric (8) are

$$2\bar{r}\phi_{,uv} + \bar{r}_{,u}\phi_{,v} + \bar{r}_{,v}\phi_{,u} = 0, \qquad (11)$$
$$-4\mathcal{A}_{,uv} - 2\kappa\phi_{,u}\phi_{,v} + \Lambda e^{\mathcal{A}} = 0, \qquad (12)$$
$$-2\bar{r}_{,uv} + \Lambda e^{\mathcal{A}}\bar{r} = 0, \qquad (13)$$
$$\bar{r}_{,uu} - 2\mathcal{A}_{,u}\bar{r}_{,u} + \kappa\bar{r}\phi_{,u}^2 = 0, \qquad (14)$$
$$\bar{r}_{,vv} - 2\mathcal{A}_{,v}\bar{r}_{,v} + \kappa\bar{r}\phi_{,v}^2 = 0. \qquad (15)$$

These are the field equations that we will use in the theory Section III below.

In 2+1 dimensions, if $\Lambda = 0$, then from (13) $\bar{r}_{,uv} = 0$. In a region containing a regular centre, one can then make the same gauge choice $\bar{r} = (v - u)/2$ as in flat spacetime. But, always in 2+1 dimensions, the coefficients of the spherical wave equation (11) depend only on $\bar{r}$, not on $\mathcal{A}$, and so the matter evolution equation is not modified by curvature. This is one intuitive way of seeing why gravitational collapse cannot occur in 2+1 with $\Lambda = 0$.

However, in the presence of a negative cosmological constant $\Lambda =: -1/\ell^2$ black holes do exist in 2+1 spacetime dimension, and can be formed from regular data. These black holes are the BTZ solutions, which in polar-radial coordinates are given by

$$ds^2 = -\left(\frac{\bar{r}^2}{\ell^2} - M\right)d\bar{t}^2 + \left(\frac{\bar{r}^2}{\ell^2} - M\right)^{-1}d\bar{r}^2 + \bar{r}^2\, d\theta^2. \qquad (16)$$

Although this looks similar to the Schwarzschild-adS solution in higher dimensions, it is locally flat. This is because in 2+1 dimensions, the Ricci tensor determines the Weyl tensor, and so a vacuum region is not only Ricci-flat but flat. The BTZ solution with $M = -1$ is the $2 + 1$-dimensionsonal adS spacetime. All other BTZ solutions with $M < 0$ have a naked conical singularity, while the BTZ solutions with $M > 0$ are black hole solutions. This mass gap between the ground state and the smallest black hole is another feature of 2+1 dimensions. Regular initial data with $-1 < M < 0$ cannot form a black hole (although they can develop arbitrarily large curvature [8].)

There seems to be a dilemma for type II critical collapse: in order to form a black hole at all, a cosmological constant is needed, but for curvature and mass scaling to occur, it must be dynamically negligible.

It is convenient to introduce the local mass function $M(u, v)$ defined by

$$M =: \frac{\bar{r}^2}{\ell^2} - (\nabla\bar{r})^2. \qquad (17)$$

This is the 2+1 dimensional equivalent of the Hawking mass for spherical symmetry in 3+1 dimensions, and has similar properties: it is constant in vacuum, while in the presence of matter it increases with $\bar{r}$ on any spacelike surface in regions where $(\nabla\bar{r})^2 > 0$. A spherically symmetric marginally outer-trapped surface (MOTS) is given by $\bar{r}_{,v} = 0$, and so its mass is given by $\bar{r}^2/\ell^2$, as is the mass of the BTZ horizon.

C. Previous work

The first numerical simulations of critical collapse of a spherically symmmetric scalar field in 2+1 dimensions with a negative cosmological constant were carried out by Pretorius and Choptuik [9] and Husain and Olivier [10].

In order to avoid the complications associated with the reflecting boundary conditions, Pretorius and Choptuik, like others in 3+1 and higher dimensions after them, focused on the scaling of maximum curvature and the mass of the apparent horizon when it first appears. They found that for each of several one-parameter families of initial data they examined, there was a p_* such that the maximum of the Ricci curvature scaled as (1) where $\gamma \simeq 1.2 \pm 0.05$. They also gave evidence for a universal CSS critical solution. They claimed also that the apparent horizon mass at first appearance scales as

$$M_{\text{FMOTS}} \sim (p - p_*)^\delta \qquad (18)$$

with $\delta = 2\gamma$, although their Figs. 4 and 5 correctly suggest a mass scaling exponent somewhere between 0 and 1. [We use the terminology FMOTS for for "first marginally outer trapped surface", as the terminology "apparent horizon mass" is ambiguous in this context; see Sec. II B 2 below.] Their theoretical argument for $\delta = 2\gamma$ is that the dimensionless mass M and area radius $\bar{r}$ of an apparent horizon are related by $M_{\text{AH}} = \bar{r}_{\text{AH}}^2/\ell^2$, and r_{AH} should scale as suggested by its dimension. We shall correct this argument in Sec. III K. Husain and Olivier found apparent horizon mass scaling with $\delta \simeq 0.81$, consistent with our results, but their data are fairly far from criticality.

On the grounds that Λ should be dynamically negligible in critical collapse, Garfinkle [11] looked for exactly CSS solutions for $\Lambda = 0$ that are analytic between the two values of x corresponding to the centre and to the past lightcone of the accumulation point (the standard procedure in higher dimensions). As we shall review in Sec. III A, he found a family of these parameterised by $n = 1, 2, 3, \ldots$. The $n = 1$ solution is the Friedmann-Robertson-Walker solution. In hindsight it is surprising that these solutions exist, as we have seen that with

$\Lambda = 0$ gravity does not affect the scalar field and so cannot regularise it, something that is essential for the existence of regular CSS solutions in higher dimensions. The Garfinkle solution is also in closed form, whereas critical solutions for spherical massless scalar field collapse in higher dimensions can only be constructed numerically (but see [12] for an existence proof of the Choptuik critical solution in 3+1 dimensions).

Garfinkle [11] noted that the $n = 4$ solution showed good agreement with the numerical data of Pretorius and Choptuik inside the lightcone. However, the lightcone is also an apparent horizon, whereas the critical solution in higher dimensions has no trapped surfaces. Furthermore, the analytic continuation of the Garfinkle solution through the lightcone has a spacelike central curvature singularity, for all n. This means that it is the CSS equivalent of a black hole, rather than a critical solution. (We will fix these problems in Secs. III B, III H, III I and III L below.)

Ignoring these obvious problems of the Garfinkle solution, Garfinkle and Gundlach [13] computed its perturbation spectrum, by making the standard requirement that perturbations be analytic at both the centre and lightcone. As we shall review in Sec. III E, they found that the Garfinkle solution with parameter n has $n - 1$ unstable modes. This then raised the problem that the $n = 2$ Garfinkle solution does not fit the numerical data, while the $n = 4$ Garfinkle solution, which does, has three growing modes. We have no theoretical solution for this problem, but we will show numerically in Sec. II C that our modified $n = 4$ Garfinkle solution appears to have only one growing mode when evolved with $\Lambda < 0$.

II. NUMERICAL RESULTS

A. Numerical method

We experimented with a time evolution code using polar-radial coordinates, the standard coordinate choice for critical collapse in higher dimensions. However, as we want to continue the evolution after the time slicing crosses the apparent horizon, we have changed over to the numerical method of Pretorius and Chopuik [9].

The metric ansatz is essentially (9), but reparameterised as

$$ds^2 = \cos^{-2}\left(\frac{r}{\ell}\right) e^{2A}(-dt^2 + dr^2) + \ell^2 \tan^2\left(\frac{r}{\ell}\right) e^{2B} d\theta^2,$$
(19)

so that

$$\mathcal{A} = A - \ln[\cos(r/\ell)], \qquad \bar{r} = \ell \tan(r/\ell) \exp B. \quad (20)$$

This brings the timelike infinity of asymptotically anti-de Sitter spacetimes to $r = \ell\pi/2$ and the centre $\bar{r} = 0$ to $r = 0$. Note that the adS spacetime is given by $A = B = 0$. We refer the reader to [9] for the field equations in these coordinates.

The metric effectively represents the metric in double-null coordinates $u := t - r$ and $v := t + r$ (which go through apparent or event horizons), but the numerical algorithm evolves it on a grid in t and r, time-stepping in t.

Both A and B obey wave equations and are evolved from initial data at $t = 0$. The residual gauge freedom is $u \to u'(u)$ and $v \to v'(v)$. We fix this in part by setting the initial data $B = B_{,t} = 0$ at $t = 0$. With ϕ and $\phi_{,t}$ also set freely, the initial data for A and $A_{,t}$ are then determined by the Hamiltonian and momentum constraints. During the evolution, we impose the gauge fixing boundary conditions $A = B_{,r} = 0$ at the adS timelike infinity $r = 1$, and the regularity boundary conditions $A = B$ and $A_{,r} = B_{,r} = 0$ at the centre $r = 0$.

The Hamiltonian and momentum constraints become singular on any time slice that contains a trapped surface, but we solve them only on the initial slice. The evolution equations remain regular at a trapped surface.

We choose units such that $G = 2$ and $\ell = \pi/2$, so that $r = 0$ represents the regular centre and $r = 1$ the adS boundary. We choose $\Delta t / \Delta r = 1/64$, and typically 4096 equally spaced grid points in r.

For a geometric analysis of the results, and in particular for looking for self-similarity near the centre, more geometric coordinates fixed at the centre are helpful. This will be discussed in Sec. II B 4 below.

B. Evolution of fine-tuned generic initial data

In scalar field critical collapse in 3+1 and higher dimensions there is a clear distinction between two outcomes. Either the scalar field forms a black hole, and the remaining scalar field escapes to infinity, or the scalar field disperses, leaving behind flat spacetime. With a negative cosmological constant, there are the twin complications that a scalar wave that disperses initially can collapse after one or more reflections at the outer boundary, and that more scalar field can fall into an initially small black hole after reflection. However, locally in space and time there are still two distinct outcomes, at least as long as the initial data are on scales much smaller than the scale ℓ set by $\Lambda = -1/\ell^2$. From now on, the previously arbitray length scale ℓ in (4) is set by the cosmological constant for definiteness. Hence $T > 0$, from (4), indicates spacetime scales smaller than ℓ.

In 2+1 dimensions, the situation appears initially more confusing. The Ricci scalar at the centre either blows up while increasing monotonically, or it goes through one or more extrema before blowing up a short time later. Similarly, the mass of the first MOTS appearing anywhere on a time slice (what [9] call the apparent horizon mass) behaves in a non-monotonic way with p.

We adopt the working definition of p_* that for $p > p_*$, $|R(0,t)|$ monotonically increases and blows up at finite t, while for $p < p_*$ it goes through at least one maximum and minimum before blowup. We shall see that with this

definition, $|p-p_*|$ controls all scaling phenomena. This is in itself an important observation, as it strongly indicates that the scaling is controlled by a single growing mode of a self-similar critical solution.

For the scalar field initial data we choose approximately ingoing (that is $\phi_{,t} = \phi_{,r}$) Gaussian or kink profiles located at $r_0 = 0.2$ with width $\sigma = 0.05$. Their amplitude p is a free parameter used for fine-tuning the initial data to the black hole threshold. Note that both chosen families of initial data are the same as considered in [9], which allows us to compare results. We find that $M_{\rm tot}(p_*) \simeq 0.003$ for both these two families. All plots and numbers presented in the current Subsection II B use the Gaussian family, but we have checked that we obtain the same results for the kink data.

The absolute value of p_* for any given one-paramter family is irrelevant and depends on the parameterisation. However, with p_* of order one, $p - p_*$ is a meaningful measure of the amount of fine-tuning. For simplicity, we use the terminology "sub10" for initial data with $p \simeq p_* - \exp(-10)$ and "super10" for $p \simeq p_* + \exp(-10)$. The best fine-tuning we have achieved is of the order of $\exp(-26)$.

1. Ricci scaling at the centre

As stated above, we define p_* so that for $p > p_*$, $|R(0,t)|$ monotically increases until blowup, while for $p < p_*$ there is at least one maximum and minimum before blowup. For subcritical data further away from criticality than approximately sub15, the Ricci scalar at the centre goes through a second maximum and minimum before blowup. Fig. 1 illustrates this for representative values of p. Going further away from criticality, the second minimum and eventual blowup moves to larger values of t. For about sub8, the blowup moves to a time $t \simeq 2.3$ that indicates one reflection from the outer boundary; see Sec. II B 3 below. Decreasing the amplitude further, below about sub7 we obtain initial data with mass below the threshold $M_{\rm tot} = 0$ for black hole formation and these data cannot form a black hole. (While we therefore cannot observe mass scaling for these data, we still observe Ricci scaling.)

The scaling of the maxima and minima of the *value* of the Ricci scalar at the centre is shown in Fig. 2. For subcritical data, the first local maximum of $|R(0,t)|$ scales as in (1) with $\gamma \simeq 1.23(4)$, the same value, to within our numerical precision, as found by [9]. We determine p_* to high precision by fitting to the Ricci scaling law (1). The critical value p_* defined in this way is consistent with the definition we have given before, but can be determined more accurately in practice.

The first minimum also scales, with $\gamma \simeq 1.4(7)$. Further away from criticality than approximately sub10, the first minimum reaches a floor set by the cosmological constant, $R \simeq 6\Lambda$. Extrapolating beyond the limit of our fine-tuning, the scaling of the first maximum and
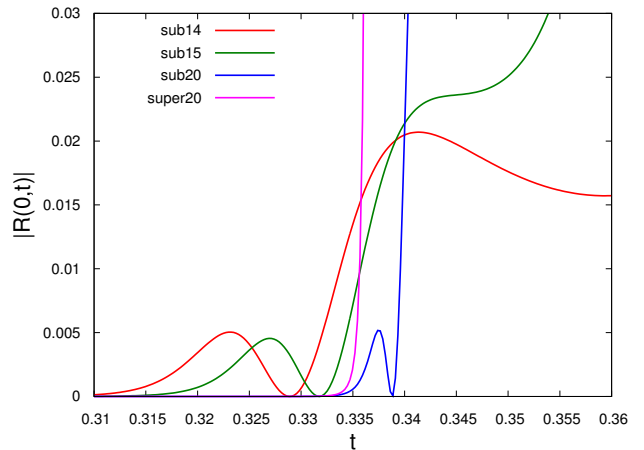

FIG. 1. $|R(0,t)|$ against t for representative values of p. The vertical axis has been rescaled to give the first maxima approximately the same value. The magenta curve super20 is for supercritical data, with immediate blowup of Ricci, while the other lines show representative subcritical data: sub20 has a maximum and minimum of Ricci followed by blowup (for $t > 0.36$), sub14 has two maxima and minima followed by blowup, and sub15 represents the transition between these last two cases, where the second maximum and minimum merge.

first minimum would suggest that they merge at sub38. However, this extrapolation is probably incorrect, as by definition we would expect them to merge precisely at $p = p_*$.

The value of the second maximum scales with $\gamma \simeq 1.17(8)$, similar to the first maximum, and the second minimum with $\gamma \simeq 1.48(9)$. At approximately sub15 its value agrees with the second maximum, and at this point the second maximum and minimum merge and disappear. The second miminum reaches the same floor as the first maximum, but only at sub2 and then at large r, which is out of the range of critical phenomena at first implosion.

Fig. 3 shows the scaling of the *locations*, in proper time at the centre t_0, of the first minimum, second maximum, and second minimum, all with respect to the first maximum, as well as the location of the first maximum with respect to the accumulation point $t_0 = t_{0*}$. The scaling exponents are 1.2(2), 1.12(7), 1.2(8) and 1.4(3) respectively, see Fig. 3. (The reason that we do not use the accumulation point as our primary reference point is that its location t_{0*} is obtained by curve-fitting, and is therefore less accurate than the location of the extrema with respect to each other.)

Checking pointwise convergence in (r,t) of our time evolutions is difficult in the critical regime because of the sensitive dependence on initial data. At best we can compare scalar quantities such as $M(x,T)$ at fine-tuning "sub$n$" for the same n at different numerical resolutions. (Note that p_* itself is resolution-dependent). This works for M and $\bar{r}$, but not for f and R. However, physical results such as Ricci and mass scaling should converge with
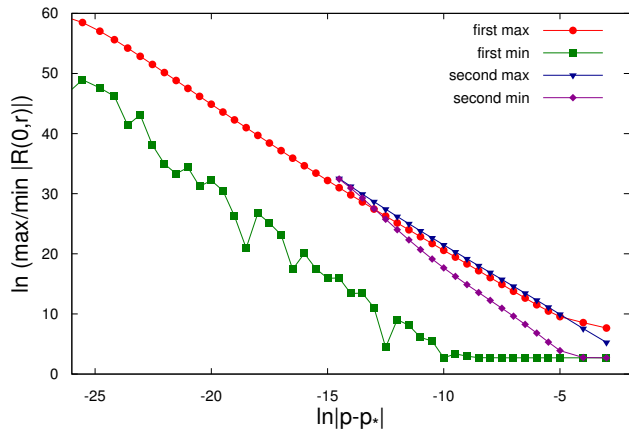
FIG. 2. Scaling of the *values* of the maxima and minima of $|R(0,t)|$. At approximately sub15, the second maximum and minimum merge and disappear, see also the sub15 curve in Fig. 1. The slope for the minima is slightly but significantly different from that for the maxima. The horizontal segments of the value of the first minimum and second minimum are dominated by the Λ term in $R = \kappa G(\nabla\phi)^2 + 6\Lambda$. The slope for the first maximum obtained by a least-square fit on the fitting interval $[-5, -26]$ is $\gamma = 1.2345 \pm 0.0076$. The standard deviation σ cited here and for similar slopes in the following is based on the hypothesis that the deviations from a straight line are independently normally distributed, and so does not take into account systematic error, which is clearly larger. However, we note that the deviation from the theoretical value of $8/7$ is 12σ or 8%.

resolution. In Fig. 4 we demonstrate that the first maximum of the Ricci scalar as a function of $\ln(p - p_*)$ converges with resolution to better than fourth order from sub3 to sub22.
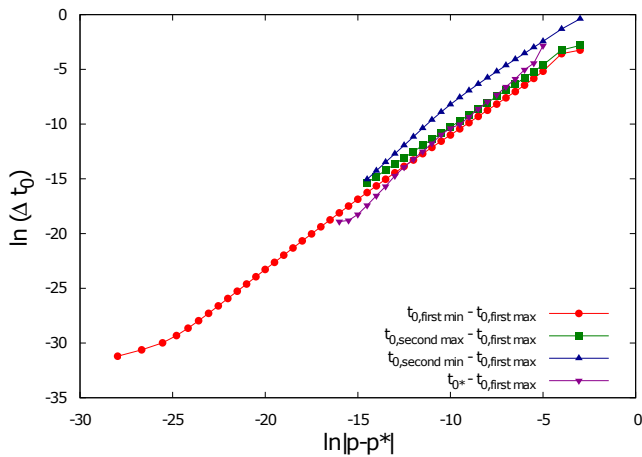

FIG. 3. Scaling of the *location* of the minima and maxima of Ricci in proper time at the centre t_0. A least-squares fit of the proper time between the first maximum and first minimum to a straight line on the fitting interval $[-5, -26]$ gives $\gamma = 1.2410 \pm 0.0067$. The fitted value differs from our theoretical value $\gamma = 8/7 \simeq 1.1429$ by 15σ, or 9%.
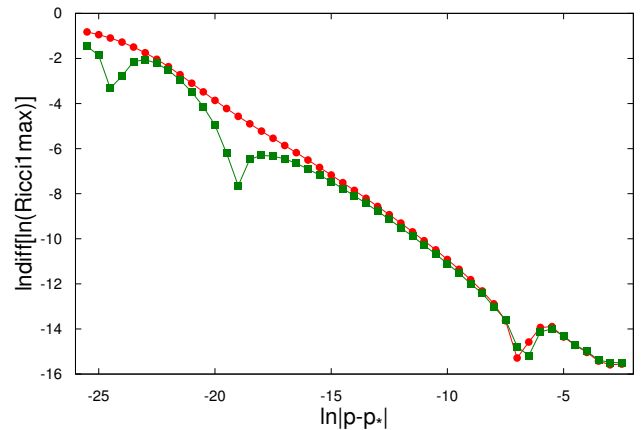

FIG. 4. Plots of $\ln(\ln R_{1k} - \ln R_{4k}) - C$ (red dots) and $\ln(\ln R_{2k} - \ln R_{4k})$ (green squares) against $\ln(p - p_*)$. Here R_{1k}, R_{2k} and R_{4k} stand for the value of the first maximum of the Ricci scalar at the centre in evolutions with 1024, 2048 and 4096 grid points, and p_* is shorthand for the relevant value for each of these resolutions, obtained by bisection. The fact that the lower resolution curve lies on or above the higher resolution curve when shifted down by $C = \ln[(4^4 - 1)/(2^4 - 1)]$ demonstrates 4-th order convergence with resolution. The value of the curves gives an estimate of $\ln$ of the numerical error in $\ln R$. The linear dependence on $\ln(p - p_*)$ is not related to the underlying scaling law, but shows that the relative error in Ricci increases with fine-tuning.

2. Apparent horizon mass scaling

The scaling argument [2] only determines the size and hence mass of the black hole when it first forms, in a regime where the transition from the critical solution to black hole formation is still universal up to an overall scale. However, in asymptotically flat spacetimes and for massless scalar field matter, little additional mass falls inlater (when the scaling argument no longer holds), so one effectively has a scaling law for the asymptotic black hole mass. (In a cosmological context, there may be significant infall [15].) In 2+1 dimensions, the cosmological constant can never be neglected where collapse takes place, and so the local scaling argument breaks down already. Furthermore, for $\Lambda < 0$ in any dimension all the mass eventually falls into the black hole because of reflecting boundary conditions. Therefore Pretorius and Choptuik focused on the mass at the first appearance (with respect to a given time slicing) of a marginally outer trapped surface (MOTS), which they call the apparent horizon mass. To explain the phenomenology we observe, we need to use a more explicit terminology, as follows.

We assume spherical symmetry. We shall use the term MOTS to denote any point (r, t) where $\bar{r}_{,v} = 0$. We shall call the union of all MOTS the apparent horizon (AH), parameterised in coordinates as a curve $t = t_{AH}(r)$. It bounds the region of outer-trapped spherically symmetric $(d-1)$-surfaces (circles in 2+1). It is easy to see using the

field equations that the AH $\bar{r}_{,v} = 0$ is spacelike for $\phi_{,v} \neq 0$ (meaning that energy crosses the horizon) and outgoing null for $\phi_{,v} = 0$. What Pretorius and Choptuik denoted by apparent horizon mass M_{AH} is the mass $M = \bar{r}^2/\ell^2$ of the first appearance of a MOTS for a given time slicing, that is the *absolute* minimum of the AH curve $t = t_{AH}(r)$ with respect to the time coordinate t. For clarity, we shall call this the first MOTS (FMOTS).

For the ingoing Gaussian data, the plot of $M_{FMOTS}(p)$ shows power-law scaling down to a very small value of M at $p = p_1 > p_*$, but then M jumps to a larger value and varies only slowly with p. This is shown in the upper plot of Fig. 6. This apparent jump is explained simply by the AH curve having two *local* minima for the range $p_* < p < p_2$, which includes p_1, see the lower plot. We shall refer to such a local minimum of $t_{AH}(r)$ as an earliest MOTS (EMOTS). It is helpful to consider the tracks of both EMOTS in the (r, t) plane (Fig. 5), together with a plot of their masses against p (Fig. 6).

At some very large value $p_0 \simeq 200$ of p (compare this to $p_* \simeq 0.133059$) there is only one EMOTS, and it is located on the initial slice $t = 0$ at some large r and M. As p is decreased from p_0, the EMOTS moves to smaller r (on track that is approximately null) and smaller $\bar{r}$ and hence M. At $p = p_2$ (approximately sub19) the single EMOTS splits into two. To the limit of our fine-tuning of the initial data, the inner EMOTS approaches zero r and M as $p \to p_*$.

For $p < p_*$, there is no inner EMOTS, and the outer EMOTS, whose mass does not scale, moves to larger r and t with decreasing p on an approximately null track, until at sub10 it approaches the outer boundary. Presumably it will then move back in, but we have not followed this further. For $p_* < p < p_1(< p_2)$ the outer EMOTS appears first, so if one looks only for the first appearance of a MOTS, for any r, its mass appears to jump at $p = p_1$ from the mass of the inner EMOTS to that of the outer EMOTS.

As far as our fine-tuning reaches, the mass of the *inner* EMOTS scales as (18) with $\delta \simeq 0.68(4)$, see Fig. 7. This value is roughly similar to the value $\delta \simeq 0.81$ of [10] (but different from the $\delta = 2\gamma \simeq 2.50$ of [9]).

As p_* is the same for both Ricci and mass scaling, to within our accuracy of fine-tuning (sub26 and super26), the exponents γ and δ must also be related. As we do not have the exact critical solution, we cannot give a complete derivation of this relation, but a tentative derivation of δ and γ based on an amended Garfinkle solution and approximate single growing mode is given below in Secs. III J and III K.

3. Second criticality

Decreasing p further, we again find critical phenomena after reflection at the outer boundary. This means that we fine-tune the amplitude such that the initially ingoing Gaussian reflects off the center, moves towards the outer
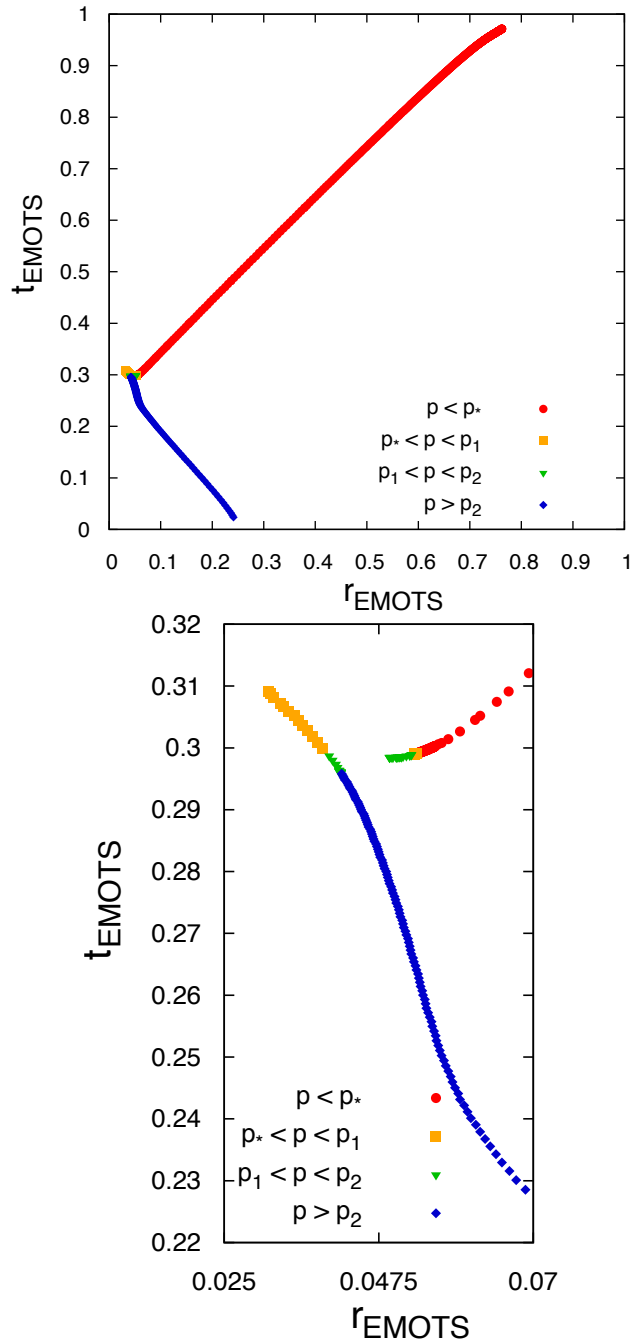

FIG. 5. Both plots show the track $[r_{EMOTS}(p), t_{EMOTS}(p)]$ of the inner and outer EMOTS. The lower plot is a closeup. Blue diamonds $(p > p_2)$ is the regime where the AH curve $t_{AH}(r)$ has only one local minimum (EMOTS), green upside-down triangles $(p_1 < p < p_2)$ the regime where there are two EMOTS but the inner one, which scales, appears first (i.e. at smaller t) and so may be considered as the FMOTS, and orange squares $(p_* < p < p_1)$ the regime where the outer EMOTS appears first. The transition between the last two regimes causes the jump in the FMOTS mass at $p = p_1$ in Fig. 6. Note that r and t are drawn to the same scale, and so radial null rays are at 45 degrees. The top right end of the subcritical (red circles) track is approximately at sub10 (corresponding also to the left edge of the upper plot in Fig. 6), but the curve does not end there.
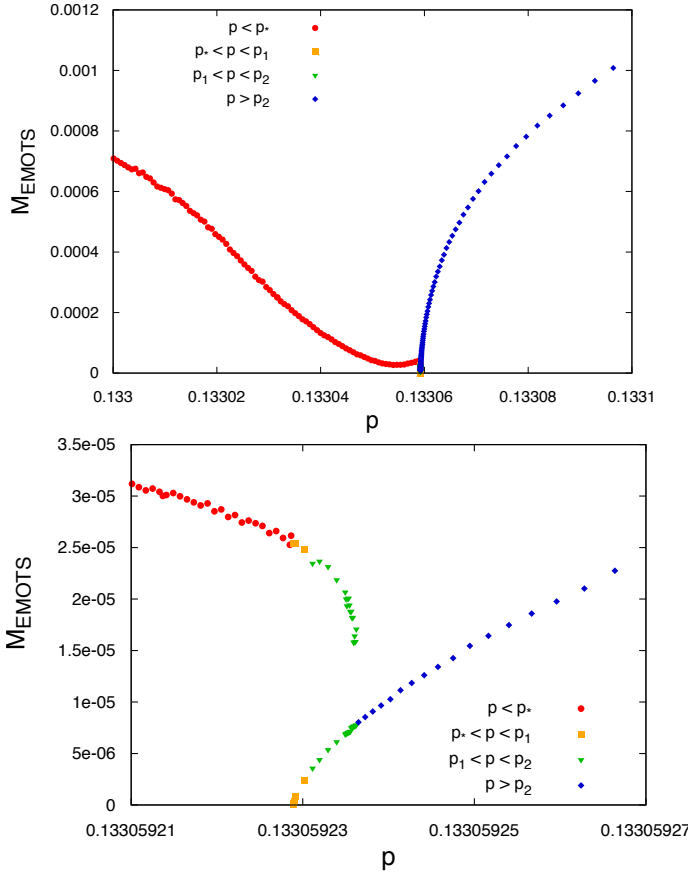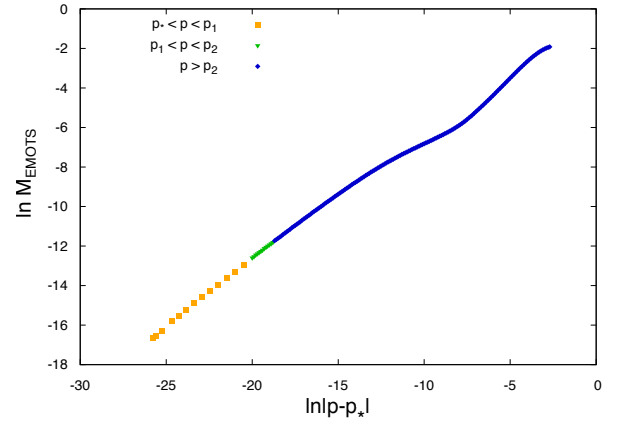
FIG. 7. Scaling of the *inner* EMOTS mass (18) with an exponent $\delta \simeq 0.6839 \pm 0.0023$, for supercritical data $p > p_*$, a deviation from our theoretical value of $16/23$ is 5σ or 2%. The colors are the same as in Fig. 5. The fitting interval is $[-26, -17]$.

FIG. 6. The top plot shows the behavior of $M_{\mathrm{FMOTS}}(p)$. At $p = p_1$, $M_{\mathrm{FMOTS}}(p)$ appears to jump to a larger value. The bottom plot is a closeup focusing on the amplitudes close to p_1. The colors and symbols for the different ranges of the parameter p are the same as in Fig. 5. In the supercritical case $p > p_*$, the only EMOTS left is the outer one, which does not scale. We expect the two curves to join at $p = p_2$, but the we cannot resolve this numerically.
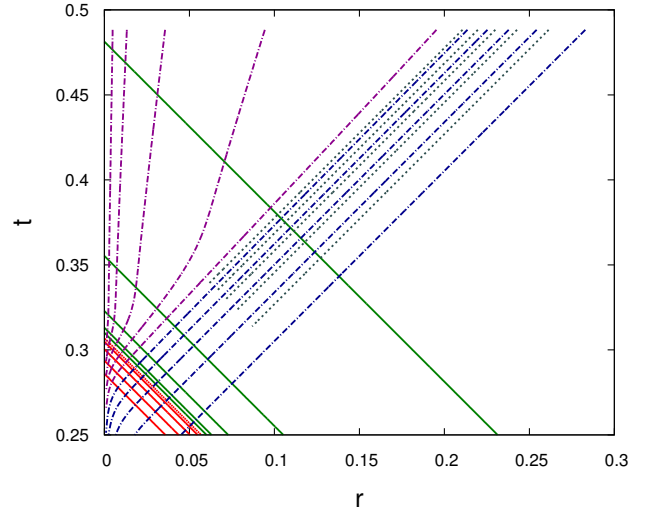

FIG. 8. Spacetime diagram of the sub10 evolution: contours of $-\ln(-\tilde{v})$ for $\tilde{v} < 0$ (red, solid lines) and of $-\ln \tilde{v}$ for $\tilde{v} > 0$ (green, solid lines), both from 9 to 13 in steps of 1, contours of $-\ln \bar{r}$ from 4 to 8 (blue, dash-dotted lines) and from 9 to 13 (magenta, dash-dotted lines) in steps of 1, and contours of $T = -\ln(-\tilde{u})$ for $\tilde{u} < 0$ from 4 to 8 in steps of 1 (gray dotted lines, shown only for $v > 0.4$ for clarity). This figure illustrates several things: the automatic zoom we get in our numerical coordinates, r and t corresponding to much smaller physical scales everywhere to the future of the accumulation point, and the transition of $\bar{r}$ from spacelike to "almost null" and back to spacelike.

boundary, reflects off it and collapses while approaching the center for the second time. The bisection is again based on the behavior of the Ricci scalar at the centre. We find that there is a second critical amplitude $p_{*1} \simeq p_{*0} - \exp(-8)$ such that the maxima and minima of the Ricci scalar for subcritical evolutions scale according to (1). This is demonstrated in Fig. 9. (We use p_{*n} to denote the critical amplitude after n reflections, with our original $p_* =: p_{*0}$.)

Note that p_{*1} is itself only sub8 with respect to p_{*0}, so that scaling maxima and minima are covered up by the initially ingoing part of the initial data. We were also unable to fine-tune as accurately as for the first criticality. At about sub20 relative to p_{*1}, the Ricci scalar still has maxima and minima, but their values fail to scale. We believe this is due to loss of numerical accuracy.

The accumulation point for immediate critical collapse, for the Gaussian initial data, was located at $t_* \simeq 0.34$ in coordinate time and $t_{0*} \simeq 0.2374$ in proper time at the centre. For critical phenomena after one reflection, for

the same family of initial data, the corresponding values are $t_{*1} \simeq 2.24$ and $t_{0*1} \simeq 0.293$. Note that the two accumulation points are separated by $\Delta t \simeq 2$, consistent with the intuitive picture of reflection at the outer boundary, but that they are separated in proper time only by $\Delta t_0 \simeq 0.05$. This is due to the fact that A and B jump down across the future lightcone of the first accumulation
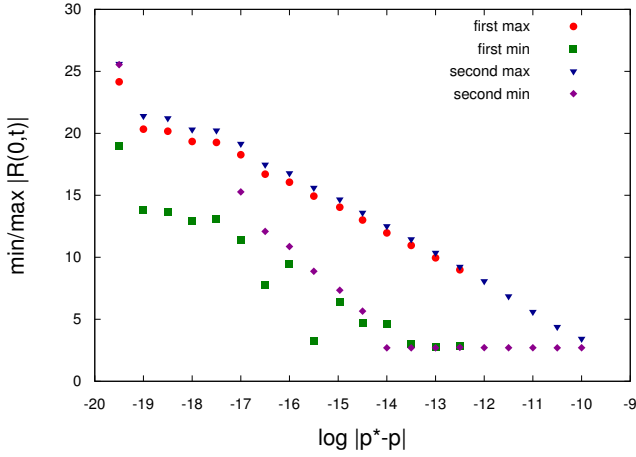
FIG. 9. Scaling of minima and maxima of $|R(0,t)|$ for subcritical evolutions with respect to the *second* critical amplitude p_{*1}. From a linear fit to the log-log plot we obtain the critical exponent $\gamma \simeq 1.065 \pm 0.44$ which is slightly different from $\gamma \simeq 1.23(4)$ obtained for p_{*0}. The fitting interval is $[-19, -12]$.
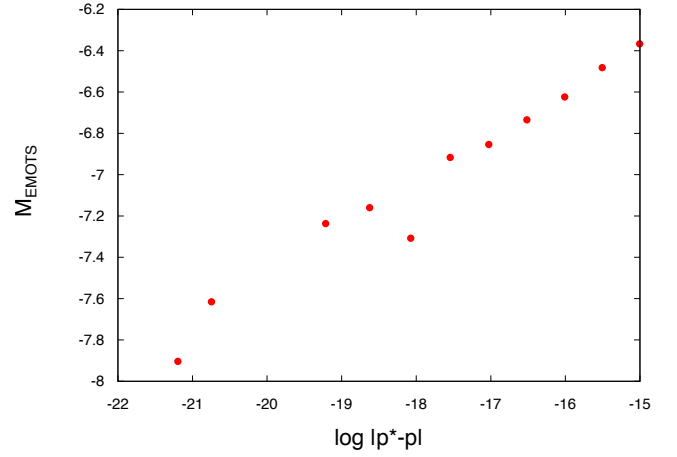

FIG. 10. The mass of the EMOTS for supercritical data after one reflection. The value of the critical exponent 0.23 found from a linear fit to the log-log plot differs from the value found for the data before any reflection. Note that p_{*1} is obtained from the second Ricci scaling, not this plot.

point to $A \sim B \sim -6$ and then remain small. Hence after first near-criticality, r and t correspond to much smaller physical scales than before, but by definition $r = 1$ is still the outer boundary and the light-crossing time is therefore still $\Delta t = 2$. See also Fig. 8 for an illustration of this memory effect in the sub10 evolution.

As a consequence of this separation of scales, the wave going back out in (first) near-subcritical evolutions comes back in what is a very short time at the centre and interacts with the aftermath of first criticality. First and second criticality therefore overlap in time, and this may explain why they are also close in p, in the sense that the scaling regimes overlap.

Furthermore, if we we compare the constant factors in front of the two Ricci scaling laws $|R|_{max} \simeq C_0(p - p_{*0})^{-2\gamma}$ and $|R|_{max} \simeq C_1(p - p_{*1})^{-2\gamma}$, we find that $C_1 \simeq 10^{-6}C_0$. This may also be a consequence of the jump down in A and B.

For second-supercritical data we also looked for evidence of mass scaling. The supercritical data with respect to p_{*1} can be also supercritical with respect to p_{*0}, and therefore to see second mass scaling one has to look at the proper range of amplitudes. We find some evidence that for second supercritical data the mass of an apparent horizon roughly behaves according to (2), but with a critical exponent $\delta \simeq 0.23$, significally different from the $\delta \simeq 0.68(4)$ found in first criticality. The evidence is presented in Fig. 10. We have no theoretical explanation of the discrepancy in the mass scaling exponent, but as the scaling appears to be very noisy anyway, the discrepancy may be just numerical error due to loss of resolution.

4. Self-similarity inside the lightcone

We now examine the claim that a CSS critical solution is observed [9], and that inside the lightcone it agrees with the $n = 4$ Garfinkle solution [11].

Recall that we denote by t_0 the proper time at the centre, starting with $t_0 = 0$ at $t = 0$. In a half-diamond bounded on the left by $r = 0$, we can rescale u and v to new double null coordinates $(\tilde{u}, \tilde{v})$, so that both correspond to $t_0 - t_{0*}$ on the central worldline $\bar{r} = 0$, which by ansatz is at $u = v$ and so is also at $\tilde{u} = \tilde{v}$, and where t_{0*} denotes the accumulation point in central proper time. A plot of the contour lines of $\ln \tilde{u}$ and $\ln \tilde{v}$ in a near-critical evolution, see Fig. 8 for sub10, shows that our numerical algorithm provides some automatic zooming in, which means we can resolve self-similarity over many e-foldings in scale without mesh refinement – to optimally resolve self-similarity, these lines should be equally spaced.

The first task is to find the accumulation point. With the scalar field at the centre in the Garfinkle solution given by $\phi(0, T) = c \ln(t_{0*} - t_0) + \text{const}$, we make a linear fit

$$\left(\frac{d\phi}{dt_0}\right)^{-1} = \frac{t_0 - t_{0*}}{c} \tag{21}$$

for c and t_{0*}. We can then compute

$$\tilde{u}(u) = t_0(u) - t_{0*}, \qquad \tilde{v}(v) = t_0(v) - t_{0*} \tag{22}$$

from $t_0(t)$ and t_{0*}. To see CSS, this needs to be done separately for each p, but t_{0*} and c depend only weakly on p and have a limit as $p \to p_*$. We have fitted $c(p)$ by the quadratic function $c(p) = c_* + c_1(p_* - p) + c_2(p_* - p)^2$. For subcritical evolutions of our Gaussian initial data, a least squares fit gives $c_* = 0.26381 \pm 0.00018$, $c_1 = 127.531$, $c_2 = -159484$ for the fitting interval $[\text{sub8}, p_*]$. This

range of c is equivalent to $n = 3.986 \pm 0.038$. Hence we can strongly rule out any n other than 4.

In the following, we denote by $\tilde{\mathcal{A}}$ the value of $\mathcal{A}$ in the preferred double-null coordinates $(\tilde{u}, \tilde{v})$. It is given in terms of the numerically evolved metric coefficient A as

$$\tilde{\mathcal{A}} = A(r,t) - \frac{1}{2}\left[A(0, t-r) + A(0, t+r)\right] - \ln[\cos(r/\ell)].$$
(23)

Following [13], we then define similarity coordinates (x, T) by

$$x := \left(\frac{\tilde{v}}{\tilde{u}}\right)^{\frac{1}{2n}}, \qquad T := -\ln\left(-\frac{\tilde{u}}{\ell}\right),$$
(24)

for n a positive integer. Hence the regular centre is given by $x = 1$ and the lightcone by $x = 0$. We also define

$$R(x, T) := \ell^{-1} e^T \bar{r},$$
(25)
$$f(x, T) := c^{-1}\phi - T - d,$$
(26)

where d is a family-dependent, dynamically irrelevant constant. The solution is then CSS if and only if $\tilde{\mathcal{A}}$, M, R, f and λ are functions of x only. These functions for the countable family of Garfinkle solution are reviewed in Sec. III A.

Finally, we define

$$\lambda := -\frac{s}{\tilde{u}},$$
(27)

where s is the affine parameter along outgoing null geodesics, measured away from the centre, and normalised so that the inner product of $\partial/\partial s$ with the 4-velocity of the central observer is -1. With the centre at $v = u$, this gives

$$s_{,v}(u, v) = \frac{1}{2}e^{2\mathcal{A}(u,v) - \mathcal{A}(u,u)},$$
(28)

which we integrate along each line of constant u. In particular,

$$s_{,\tilde{v}}(\tilde{u}, \tilde{v}) = \frac{1}{2}e^{2\tilde{\mathcal{A}}(\tilde{u}, \tilde{v})}.$$
(29)

The rescaled

$$\bar{\lambda}(x) := \lambda(x)/\lambda(0)$$
(30)

is a function of x only in CSS, and having tested this, we will later use it as the similarity coordinate in place of x.

Fig. 11 shows a comparison of the mass function $M = M_G(x)$ of the Garfinkle solution with $n = 4$ against $M[x(r,t), T(r,t)]$ of the sub25 evolution. There is good agreement everywhere between the regular centre and the lightcone ($0 \leq x \leq 1$), over the range $6 \leq T \leq 14$, which means that the solution is CSS inside the lightcone over 8 e-foldings of scale, all of which are much smaller than the scale ℓ set by the cosmological constant. Fig. 12 shows a similar comparison of $f_G(x)$, against $f[x(r,t), T(r,t)]$,
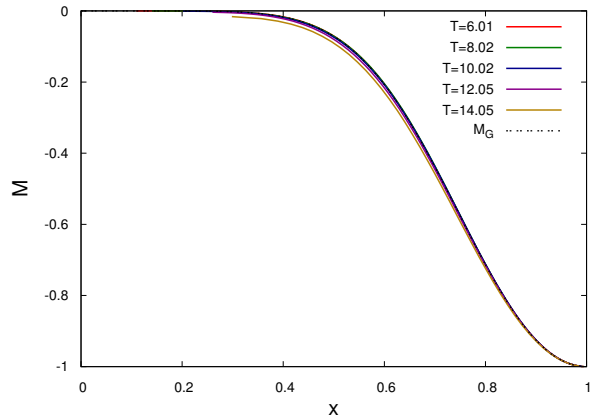

FIG. 11. Comparison of the mass function $M[x(r,t), T(r,t)]$ in the sub25 evolution at five $T = \text{const}$ moments against the $n = 4$ Garfinkle solution $M_G(x)$. The numerical data are plotted for $T = 6.01$ (red), $T = 8.02$ (blue), $T = 10.02$ (magenta), $T = 12.05$ (gray) and $T = 14.05$ (orange). The Garfinkle solution is denoted by a dotted black line. The ℓ^2 norm of the difference between numerical results and the Garfinkle solution for $n = 4$ calulated for $T = 10.02$ is 0.013. This norm is around 60 times larger for $n = 3, 5$ and over 200 times larger for $n = 2, 6$.
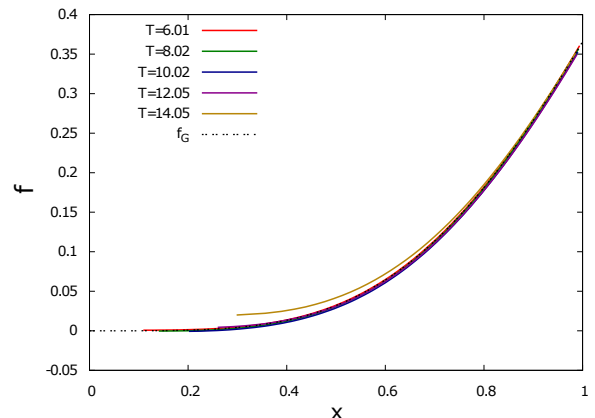
FIG. 12. Comparison of the $f[x(r,t), T(r,t)]$ in the sub25 evolution given at five $T = \text{const}$ moments with $f_G(x)$. Even more clearly than by the comparison of f against f_G, $n = 3$ and $n = 5$ are ruled out by our estimate of n from the cT dependence of $\phi(r,t)$.

where the constant d depends on the family of initial data (but not on p) and has been determined by fitting. Figs. 13 and 14 show the corresponding tests for R and $\bar{\lambda}$.

Even though there is good numerical evidence that the critical solution inside the lightcone is the $n = 4$ Garfinkle solution (up to small corrections in powers of Λ), we keep n generic in the following for clarity of presentation.

FIG. 13. Comparison of $R[x(r,t), T(r,t)]$ in the sub25 evolution against $R_G(x)$. Again, the numerical data are given at five $T = \text{const.}$ moments.
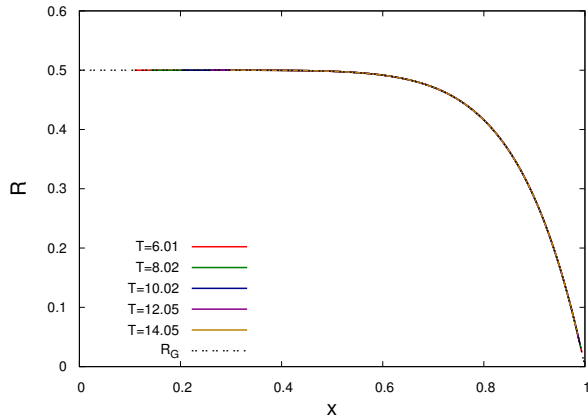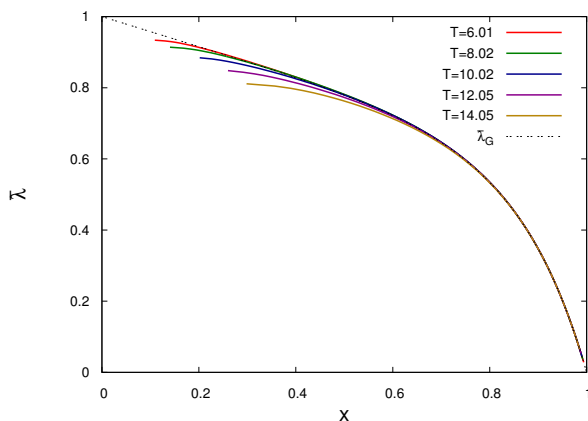

FIG. 14. Comparison of $\bar{\lambda}[x(r,t), T(r,t)]$ in the sub25 evolution inside the lightcone for five moments of T against $\bar{\lambda}_4(x)$.

5. Outside the lightcone

Garfinkle [11] compared his exact solution with the numerical evolutions of [9] only inside the lightcone. Here we will go significantly beyond the lightcone. We will see that the analytic continuation of the Garfinkle solution is definitely ruled out, but that a different, C^3, continuation proposed in Sec. III B below, and which we call the null continuation, appears to be at least a rough approximation to the true critical solution.

The best choice of data for this comparison would appear to be an evolution with the best available fine-tuning, as there we expect to see the critical solution most clearly. However, in near-critical evolutions, even subcritical ones, the evolution ends in a central singularity very soon after the accumulation point of the CSS regime. This is different from critical collapse in 3+1 and higher dimensions, where subcritical evolutions go to essentially vacuum after the CSS regime (in the case $\Lambda < 0$, at least until the next reflection at the outer boundary). Hence we also consider the sub10 evolution, which cor-

responds to the closest we can get to critical initial data while still having a significant evolution in t after the accumulation point of the CSS region. In sub10, we have access to large positive values of $v = t - r$, but because A and B are very negative in this regime, this does not correspond to large values of the proper retarded time $\tilde{v}$ or area radius $\bar{r}$, and so we are not far away in this sense from the accumulation point. See again Fig. 8 in this context.

Recall that $\tilde{v}$ is normalised to proper time at the regular centre, so it is not defined outside the past of blowup at the centre. Moreover, even in subcritical evolutions, where blowup occurs significantly after the accumulation point, spacetime at the centre after the accumulation point is not expected to be self-similar. Hence we cannot use the similarity coordinate x based on $\tilde{v}$ and $\tilde{u}$ outside the lightcone of the critical solution. We use $\bar{\lambda}$ instead. It is given in terms of x for both the Garfinkle solution and its null continuation in Sec. III C below.

Fig. 15 shows contour lines of T, $\bar{\lambda}$ and x in the (r,t) plane for the sub25 evolution with singularity excision. Near the center the contour lines of x and λ are approximately parallel, as one would expect in a CSS spacetime. Near the lightcone, they are not even approximately parallel, and the contour line $\bar{\lambda} = 0$ is not particularly close to the past lightcone of the accumulation point. (The contour line $x = 0$ is precisely the past lightcone of the accumulation point by definition.) This disagreement is already visible in Fig. 14, but appears more clearly here because both x and $\bar{\lambda}$ vary very slowly with respect to t and r near the lightcone. We believe that the origin of the discrepancy is that the true critical solution has a symmetry that is approximately CSS only inside the lightcone, but changes over to a different symmetry outside the lightcone in analytic manner; see Sec. III L below. Hence we expect some deviation from CSS already as we approach the lightcone from the inside.

Fig. 19 shows contour lines of T, $\bar{\lambda}$ and x for the sub10 evolution. The discrepancy between x and λ is visible here, too. Sub25 gives us the larger range of T (better fine-tuning), while sub10 gives us the larger range of $\bar{\lambda}$ (larger t before the simulation stops). Overlaying the two sets of T and $\bar{\lambda}$ contour lines in Fig. 20 shows that the T contours are essentially the same, while the $\bar{\lambda}$ contours differ significantly for $T \gtrsim 6$, as does the coordinate location of the accumulation point. Yet when we plot M, R and f against $(\bar{\lambda}, T)$, the two evolutions agree perfectly with the Garfinkle solution, and therefore each other, inside the lightcone.

By comparing M, f and R with the null-continued Garfinkle solution, Figs. 16-18 for sub25 and Figs. 21-23 for sub10 also demonstrate that the analytic continuation is clearly ruled out, while the null continuation appears more plausible. In sub10, the strongest indication of this is that $M \simeq 0$ outside the lightcone, while the evidence from R and f is somewhat less clear.

Our plots of M, R and f against $\bar{\lambda}$ or x, at a range of fixed values of T, show that inside the lightcone the
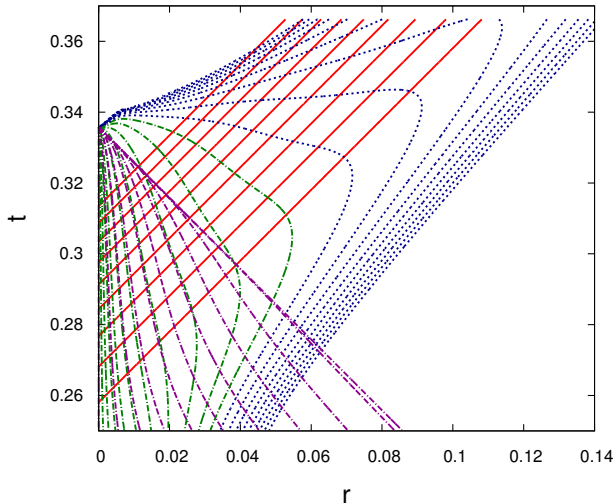
FIG. 15. Contour lines of T from 6 to 14 (red, solid) in steps of 1, contour lines of $\bar{\lambda}$ from 0 to 1 (green, dash-dotted) and from 1.1 to 2 (blue, dotted) in steps of 0.1 and contour lines of $x(r,t)$ (magenta dash-dotted for $1 \geq x \geq 0$ in steps of 0.1) in the sub25 evolution. Excision allows us to access a wider range of $\bar{\lambda}$ for $6 < T < 14$. (Excision begins at the centre at $t = 0.34$ and spreads to $r = 0.05$ before the evolution stops at $t = 0.365$.) The contour lines of x and $\bar{\lambda}$ are approximately parallel near the centre, but not near the lightcone. This is clearer here than in Fig. 14 based on the same data. Note that while $\bar{\lambda} = 1$ is approximately null for $6 < T < 14$, it is significantly to the future of the past lightcone $x = 0$ of the accumulation point.
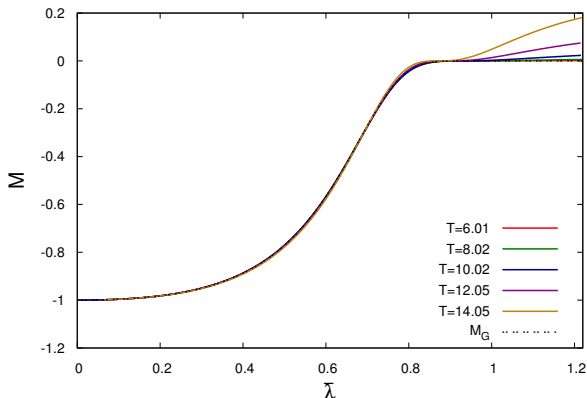

FIG. 16. $M(\bar{\lambda}, T)$ in the sub25 evolution with excision for five values of T in the interval $[6, 14]$.

deviations from the $n = 4$ Garfinkle solution are very small. Such deviations are expected from a number of sources. In Sec. III H below we compute perturbative corrections to the Garfinkle solution for a nonvanishing $\Lambda < 0$. These are of order $\Lambda \tilde{u}^2 = \exp{-2T}$ and hence very small. We also expect one growing perturbation, which is small by virtue of fine-tuning, infinitely many decaying perturbations, small by virtue of large T, and numerical error. As these deviations from the Garfinkle solution are unlikely to cancel systematically, our plots
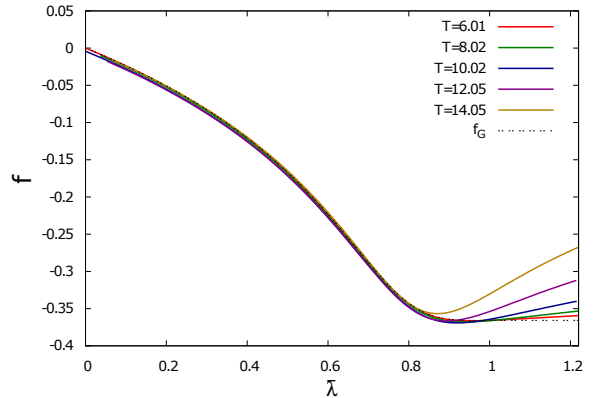

FIG. 17. $f(\bar{\lambda}, T)$ in the sub25 evolution with excision for five values of T.
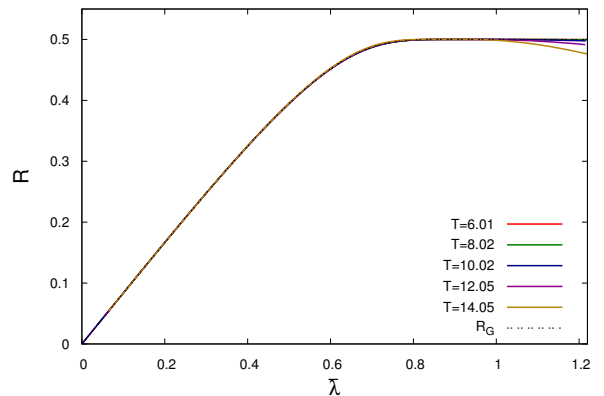
FIG. 18. $R(\bar{\lambda}, T)$ for $6 < T < 14$ in the sub25 evolution with excision for five values of T.

indicate that they are all separately small.

Outside the lightcone, the deviations from our proposed null continuation of the $n = 4$ Garfinkle solution are larger than inside the lightcone. It is clear that they cannot be mainly Λ corrections, as they increase with T, rather than depending on T as $\exp{-2T}$. Rather, we believe that these deviations depend on the initial data in a manner that does not vanish in the fine-tuning limit. Mathematically, this may reflect that the discrete perturbation modes of the critical solution are not complete, or that a sum over those modes does not converge outside the lightcone. The latter could happen because individual modes that decay more rapidly with T grow more rapidly as functions of x outside the lightcone. (While we formally construct the discrete mode spectrum in Sec. III E below, we have only explicitly calculated the growing modes as functions of x.) Yet another way of looking at this is to note that while demanding CSS and analyticity at the centre and the lightcone uniquely defines the countable family of Garfinkle solutions, the null data on the lightcone define a unique analytic continuation only if we demand CSS everywhere.

In Sec. III L below, we find an ODE system whose solution is an exact solution of the full field equations for

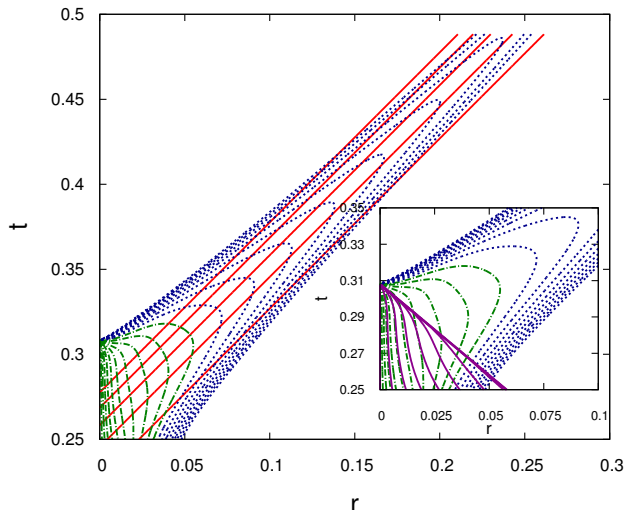FIG. 19. Contour lines of T from 4 to 8 (red, solid) in steps of 1, and contour lines of $\bar{\lambda}$ from 0 to 1 (green, dash-dotted) and from 1.1 to 2 (blue, dotted) in steps of 0.1, in the sub10 evolution. The code stops much later than in the sub25 evolution, allowing us to access a much larger range of $\bar{\lambda}$. The inset shows again contour lines of $\bar{\lambda}$ (colours and lines as in the main plot), and contour lines of x for $0 \leq x < 1$ (magenta, solid).
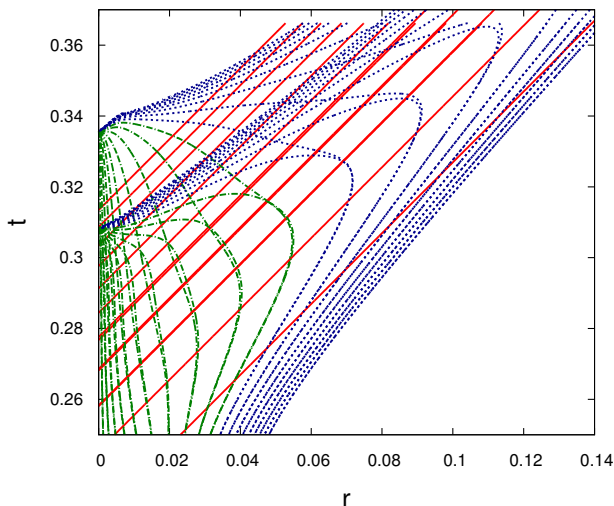
FIG. 20. Overlay of Figs. 15 (sub25) and 19 (sub10), but without the contour lines of x. The T contour lines (from 6 to 14 for sub25 and 4 to 8 for sub10) essentially agree. The $\bar{\lambda}$ contour lines agree for $T \lesssim 6$. The coordinate time value t_* of the accumulation point differs significantly between the two evolutions (0.31 and 0.34). (The proper time value t_{*0} is essentially the same.)

finite $\Lambda < 0$ outside the lightcone, and which can be matched at the lightcone to the Garfinkle solution and its first Λ corrections as smoothly as the null continuation itself, namely C^3. Hence, this is better than the null continuation plus Λ corrections, but one may wonder how the two are related. As discussed in Sec. III B
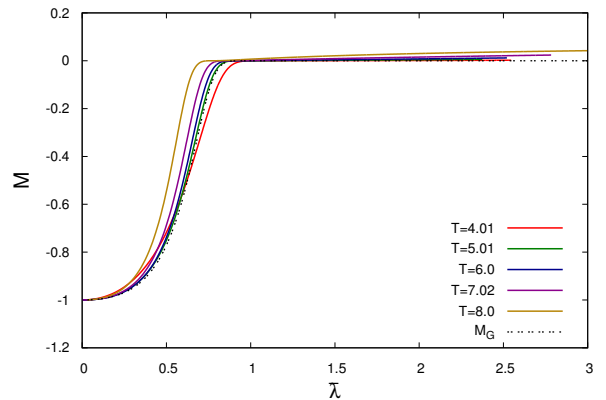
FIG. 21. $M(\bar{\lambda}, T)$ for the sub10 evolution. In the analytic null continuation of the Garfinkle solution, $M(1 - \bar{\lambda}) = -M(\bar{\lambda})$, whereas in the null continuation $M(\bar{\lambda}) = 0$ for $\bar{\lambda} > 1$. Clearly the latter fits the plot and the former does not.
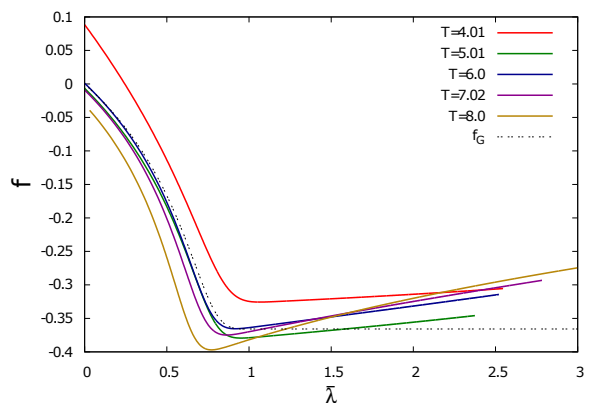
FIG. 22. $f(\bar{\lambda}, T)$ for the sub10 evolution.
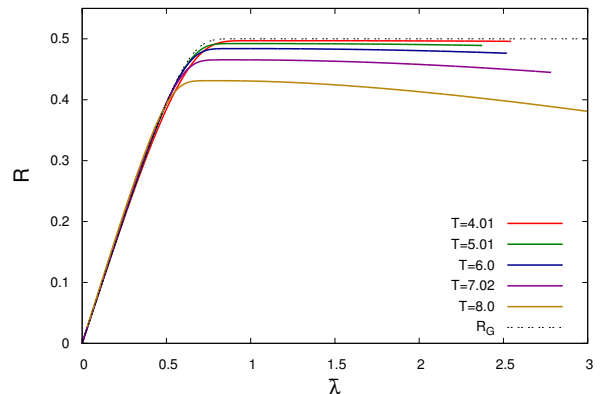
FIG. 23. $R(\bar{\lambda}, T)$ for the sub10 evolution. In the analytic null continuation of the Garfinkle solution, $R(1 - \bar{\lambda}) = R(\bar{\lambda})$, whereas in the null continuation $R(\bar{\lambda}) = 1/2$ for $\bar{\lambda} > 1$. Clearly the latter fits the plot better than the former.

below, the bare null continuation has a null translation invariance in addition to spherical symmetry and CSS. Our exact outer solution has only one continuous symmetry of a hitherto unknown type: it acts as an isometry

on the (r, t) plane but a CSS on the orbits of spherical symmetry. However, if we expand this solution into a series in powers of $\exp -2T$, we obtain term by term the null continuation and its perturbative Λ corrections, so we can also think of it as an approximate CSS symmetry. (Recall that with finite Λ, exact CSS is impossible.) In the regime where we have plotted near-critical solutions, even the first-order Λ corrections are very small compared to the zeroth order null continuation, so the deviations from the null continuation that we see cannot be caused mainly by these. For the same reason, we cannot distinguish the null continuation plus first Λ correction from the exact solution of which it is the expansion.

C. Evolving initial data for our amended Garfinkle solution

1. Motivation and overview

Our working hypothesis, compatible with the numerical results presented so far, is that there is a true critical solution, which is asymptotically CSS, and which has one growing mode with $\lambda_0 \simeq 7/8$. We have given strong numerical evidence that this critical solution is very well approximated by the $n = 4$ Garfinkle solution inside the lightcone. We have also given, somewhat weaker, numerical evidence that outside the lightcone it is approximated not by the analytic continuation of the Garfinkle solution, but by what we have called its null extension.

The $\Lambda = 0$ Garfinkle solution has a MOTS on its lightcone, and the $\Lambda = 0$ null extension has a MOTS at every point. Therefore, on theoretical grounds, we need to add a Λ correction to both, which removes the MOTSs. (These corrections are de facto so small, at least inside the lightcone, that we would have no reason to add them only to improve agreement with our numerical data.) We shall call this null-continued, Λ-corrected $n = 4$ Garfinkle solution the "amended Garfinkle solution".

Our amended Garfinkle solution still has two obvious shortcomings, namely that both it and its linear perturbations are not analytic but only C^3 at the lightcone, and that it has three growing modes. Analyticity at the lightcone is a natural requirement if the critical solution is required to arise from the evolution of generic initial data. Hence the non-analyticity is not a mere technical shortcoming, and may well be related to the incorrect number of growing modes. Similarly, any universal critical solution can only have one growing mode.

In this Subsection we will give numerical evidence that, in some way that we do not yet understand theoretically, these twin problems seem to cancel each other out. We shall evolve initial data for our amended Garfinkle solution, matched outside its lightcone to asymptotically adS data, and add perturbations from one of five families: two that we consider as generic, and the three growing perturbation modes of the null-continued $n = 4$ Garfinkle solution. We shall find that these data evolve in the

expected CSS way, and that our amended Garfinkle solution with (approximately) zero perturbation is critical in all of these five families, showing scaling with $\gamma \simeq 8/7$ and $\delta \simeq 16/23$ in each case, with no indication of any other growing mode. Hence we conclude that analyticity and the presence of the cosmological constant together somehow suppress the $\lambda = 2/8$ and $3/8$ growing modes, while the top $7/8$ mode survives.

2. Data and results

The technical details of how we construct the initial data at $t = 0$ for our amended Garfinkle solution are given in Sec. III M below. Here we need to say only that they are parameterised by T_{initial}, the value of T at $(r = 0, t = 0)$, which governs the magnitude of the Λ corrections, the value $r_{\mathrm{lightcone}}$ of r where the lightcone of the Garfinkle solution intersects $t = 0$, and the location r_0 and width Δr of the switchover from Garfinkle data to vacuum.

We have chosen $T_{\mathrm{initial}} = 10.0$ in order to make the Λ correction small throughout the initial data, and $r_{\mathrm{lightcone}} = 0.3$, $r_0 = 0.6$ and $\Delta r = 0.3$ in order to minimise spurious mass generated by the switching. With these parameters the total mass is 0.00635. The Λ correction to the initial data is small enough not to be visible in plots, and is of course expected to decay further as $\exp(-2T)$. Hence we can expect to compare the time evolution of these data against the null-continued $\Lambda = 0$ Garfinkle solution within our plotting accuracy.

In the first one-parameter family of deformations of these data, we multiply $\phi(r, 0)$ and $\phi_{,t}(r, 0)$ by a factor of $1 + p$. We find that the critical value is $p_* \simeq 6.68 \cdot 10^{-7}$. As expected, this is small. Moreover, we find good agreement with the $n = 4$ Garfinkle solution inside the lightcone from $t = 0$ onwards, as there is no transition from generic initial data to the Garfinkle solution.

We find that $M \simeq 0$, $f \simeq 2 \ln 2$ and $R \simeq 1/2$ outside the lightcone, as they would be in the null continuation. This is demonstrated for the sub8 evolution in Figs. 24-26. (We do not know why the deviation in f is relatively much larger). We have chosen sub8 because it is in the middle of the range of $\ln(p_* - p)$ where we see convergence of the Ricci scaling, and hence trust our evolution.

With the same fitting procedure we used above for Gaussian initial data, a fit of $c(p)$ for subcritical $(1 + p)$-times-Garfinkle data gives $c_* = -0.263871 \pm 1.7 \cdot 10^{-10}$, $c_1 = -0.263861$ and $c_2 = 5.502 \cdot 10^{-5}$ for the fitting interval $[\mathrm{sub}3, p_*]$. This is equivalent to $n = 3.999036 \pm 3.7 \cdot 10^{-8}$. The values of constants c_1 and c_2 are much smaller than for Gaussian initial data, meaning that c depends only very weakly on p. Clearly, the formal fitting error is an overoptimistic estimate of the error in n, but the evidence strongly suggests $n = 4$ again.

In a second 1-parameter family of initial data, we take our best approximation to the critical point of the first family and add a Gaussian (centre 0.2, width 0.05) in ϕ
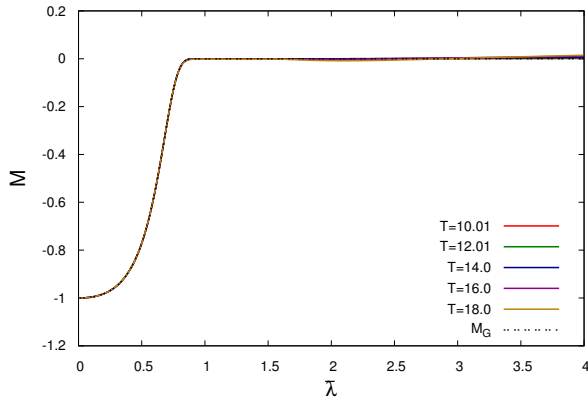
FIG. 24. $M(\lambda, T)$ for evolution of sub8 Garfinkle initial data for five chosen moments of $T = $ const., where the scalar field is multiplied by the factor $1 + p$.
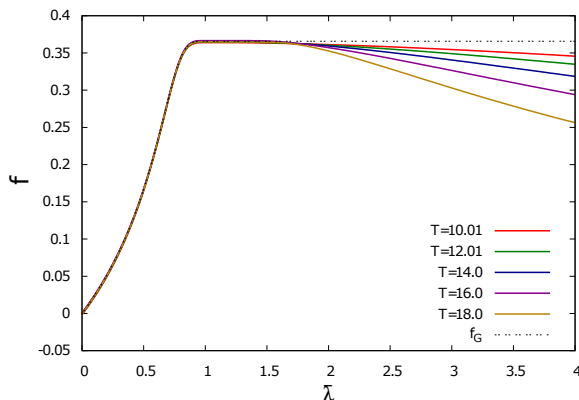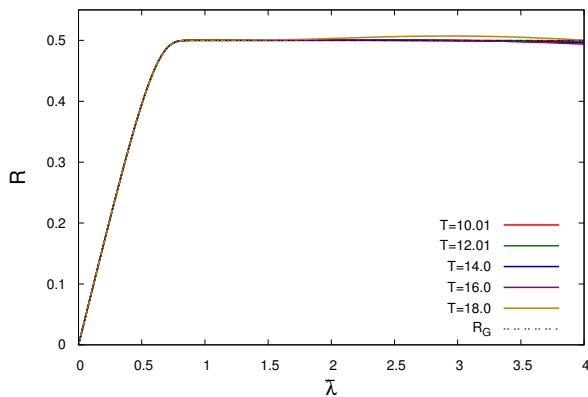

FIG. 25. The same for $f(\lambda, T)$.

FIG. 26. The same for $R(\lambda, T)$.

and $\phi_{,t}$ with overall amplitude p. The critical value for this family is $p_* \simeq 5.5 \cdot 10^{-10}$. We would expect this to be very small, as the $p = 0$ element of this family is already our best approximation to the critical point of the first family.

We have created three other 1-parameter families of initial data by adding one of the $m = 7$, $m = 3$, and $m = 2$ growing perturbations of the null-extended Garfinkle

solutions to the best fine-tuned data of the first family. We add the perturbations for both ϕ and B and their derivatives, with $c_2 = p$, and then solve the (nonlinear) constraints for A and $A_{,t}$. The critical values are $p_* = 5.5 \cdot 10^{-9}$, $5.5 \cdot 10^{-12}$ and $5.5 \cdot 10^{-14}$.

All five families show similar subcritical power-law scaling of the values and proper time locations of the extrema of the Ricci scalar at the centre. This is demonstrated in Figs. 27-29 for the first family. The value of γ obatained for this family is compatible, within our numerical accuracy, with the theoretical value $\gamma = 8/7$ and slightly different from the result obtained for Gaussian initial data. However, the discrepancy is not significant if we take into account that the actual deviation of our data from a straight line is not random but smooth (i.e. systematic). By eye, a straight line with slope $8/7$ seems to be as good a fit as the least-squares straight line. That the deviation from $8/7$ is smaller than for the Gaussian initial data might be explained by the fact that for our approximate critical solution we start much closer to the true critical solution, and less fine-tuning is needed to observe the scaling.
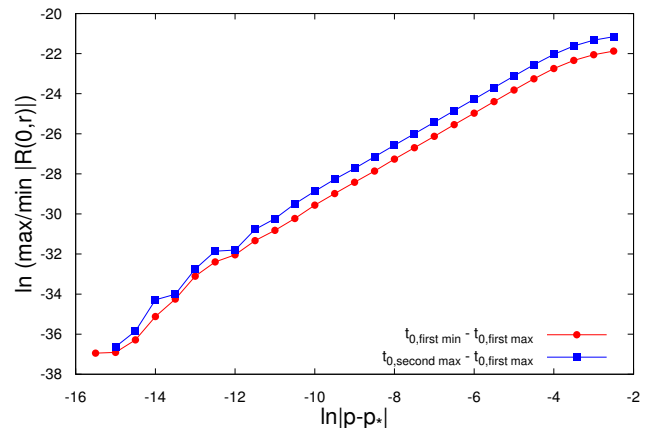
FIG. 27. Log-log plot of the proper time of the first minimum and second maximum in Ricci at the centre, relative to the first maximum, against $p - p_*$, for our "amended Garfinkle solution" initial data, with the scalar field initial data scaled by $1 + p$. From a fit on the interval $[-11, -4]$ to the first maximum we find $\gamma = 1.1441 \pm 0.0022$, compatible with $\gamma = 8/7$.

We have also looked at mass scaling for the supercritical evolutions. At low fine-tuning, for example from super5 to super15 for the $m = 7$ family of initial data, we find a MOTS present already in the initial data. (To be precise, our initial data constraint solver fudges the MOTS, but it then appears on the first time step.) At larger fine-tuning, say for super17 to super27 for this family, the EMOTS occurs at some $t > 0$. We find that the mass of the MOTS in the initial data, or the EMOTS forming later, lie on a single curve with $\delta = 16/23$. In Sec. III K, where we derive δ, we explain why it also applies for the MOTS in the initial data in this case. The mass scaling for Garfinkle family of initial data is pre-

Family of initial data	γ	fitting interval	δ	fitting interval
Gaussian	1.2345 ± 0.0076	[-26,-5]	0.684 ± 0.023	[-26,-17]
$(1+p)$Garfinkle	1.1441 ± 0.0022	[-11,-4]	0.6684 ± 0.0017	[-14,-3]
$(1+p_*)$Garfinkle+Gauss. pert.	1.1402 ± 0.0056	[-18,-10]	0.6765 ± 0.0018	[-19,-9]
$(1+p_*)$Garfinkle $+ m = 2$ pert.	1.1234 ± 0.0031	[-18,-10]	0.6894 ± 0.0076	[-19,-8]
$(1+p_*)$Garfinkle $+ m = 3$ pert.	1.1442 ± 0.0084	[-20,-10]	0.6730 ± 0.0021	[-20,-11]
$(1+p_*)$Garfinkle $+ m = 7$ pert.	1.14290 ± 0.00044	[-25,-13]	0.6991 ± 0.0033	[-25,-10]
Theoretical values	$8/7 \simeq 1.1429$		$16/23 \simeq 0.6957$	

TABLE I. Values of γ and δ obtained in fitting power laws to the maximum of Ricci and mass of the (inner) EMOTS together with error bars and fitting intervals (in $\ln|p-p_*|$). Some fitting intervals were chosen not according to the convergence results, but were modified due to the fact that scaling started for more critical data.
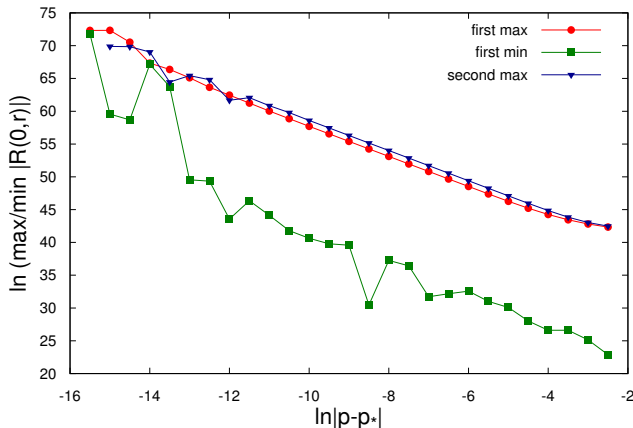
FIG. 28. Scaling of the values first and second maxima and first minimum of $|R(0,t)|$, for the same initial data. From fit in the same interval as for the figure above, we have $\gamma = 1.1432 \pm 0.0073$, which is again compatible with theoretical value $\gamma = 8/7$.
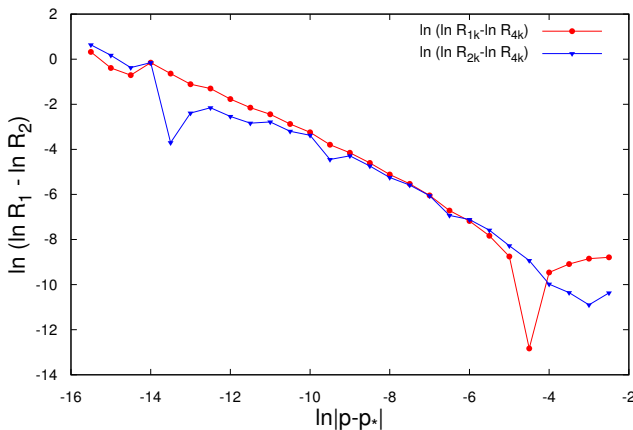
FIG. 29. Convergence of the first maximum of Ricci as a function of $p - p_*$, similar to Fig. 4 but now for the (null-continued, Λ-corrected) Garfinkle data, fine-tuned by rescaling the scalar field initial data by an overall factor of $(1+p)$. In contrast the fine-tuned Gaussian data in Fig. 4, here $C = \ln[(4^1 - 1)/(2^1 - 1)]$, demonstrating 1st-order order convergence with resolution.

sented in Fig. 30.

The $(1+p)$-times-Garfinkle family of initial data shows first-order convergence in the intervals [sub4, sub14] (see Fig. 29) and [super3, super14]. For fine-tuned Garfinkle initial data plus a Gaussian perturbation we also see first-order convergence in the intervals [sub5, sub22] and [super5, super19]. For subcritical evolutions of $m = 2$ perturbations of the Garfinkle data we observe second-order convergence in the interval [sub5, sub22] and first order-convergence for supercritical data in the interval [super3, super19]. For $m = 3$ perturbations we again have first-order convergence in the intervals [sub6, sub21] and [super2, super20]. $m = 7$ perturbations show second-order convergence for subcritical evolutions in the inter-
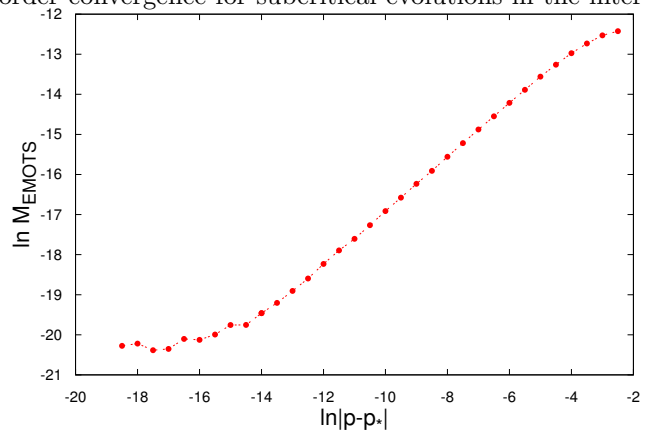
FIG. 30. Scaling of the EMOTS mass for supercritical evolutions of $(1 + p)$-times-Garfinkle initial data. The fit in the interval [-14,-4] gives $\delta = 0.6684 \pm 0.0017$, which is 16σ or 4% below the theoretical value $16/23$.

val [sub7, sub15] followed by first-order convergence in [sub15, sub25], while for supercritical evolutions the convergence is first order in the interval [super3,super25]. The results obtained in fitting γ and δ to the power laws for all families of initial data studied are given in Table I.

III. THEORY

A. The Garfinkle solution

This Subsection is based on [11] and is included here for completeness. In the metric coefficients $\tilde{\mathcal{A}}$ and R and coordinates (x, T) defined in (23-25), the general metric becomes

$$ds^2 = \ell^2 e^{-2T} \left[e^{2\bar{\mathcal{A}}} \left(dx - \frac{x}{2n} dT \right) dT + R^2 \, d\theta^2 \right], \quad (31)$$

where we have defined the shorthand $\bar{\mathcal{A}}$ by

$$e^{2\bar{\mathcal{A}}} := 2nx^{2n-1} e^{2\tilde{\mathcal{A}}}. \quad (32)$$

In order to eliminate κ from the field equations (10), we define the positive dimensionless parameter $\tilde{c}$ from the dimensionful parameter c by

$$\tilde{c} := \sqrt{8\pi G c^2}. \quad (33)$$

The Garfinkle solution [11] of the field equations (10) with $\Lambda = 0$, denoted by the subscript 0, is then given by

$$e^{2\tilde{\mathcal{A}}_0} = \left(\frac{1 + x^n}{2} \right)^{4\tilde{c}^2} x^{-2n\tilde{c}^2}, \quad (34)$$

$$R_0 = \frac{1 - x^{2n}}{2}, \quad (35)$$

$$\phi_0 = c \left[T - 2\ln\left(\frac{1 + x^n}{2} \right) \right]. \quad (36)$$

The mass function is given by

$$M_0 = -\left(\frac{1 + x^n}{2} \right)^{-4\tilde{c}^2} x^{2n-1}, \quad (37)$$

which takes value $M = -1$ at the centre, as necessary for regularity, and $M = 0$ at the lightcone.

So far, the Garfinkle solution is analytic at the centre $x = 1$ for any $\tilde{c}$ and any positive integer n, but it is generically singular at the lightcone $x = 0$, because $\exp 2\bar{\mathcal{A}}_0$ is either zero or infinite there. However, with

$$\tilde{c}^2 = 1 - \frac{1}{2n}, \quad (38)$$

the overall power of x in $\exp 2\bar{\mathcal{A}}$ cancels and the solution is also analytic at the lightcone $x = 0$, with

$$e^{2\bar{\mathcal{A}}_0} = 2n \left(\frac{1 + x^n}{2} \right)^{4\tilde{c}^2}. \quad (39)$$

Hence, the Garfinkle solution is analytic at the centre and lightcone if and only if $n = 1, 2, \ldots$, thus restricting the possible values of c.

In order to give an analytic form of the metric also in double null coordinates, we rescale $\tilde{v}$ to something that is proportional to x, namely [11]

$$\hat{v} := -\ell \left(-\frac{\tilde{v}}{\ell} \right)^{\frac{1}{2n}} \quad \Rightarrow \quad x = \left(-\frac{\hat{v}}{\ell} \right) \left(-\frac{\tilde{u}}{\ell} \right)^{-\frac{1}{2n}}. \quad (40)$$

The metric then becomes

$$ds^2 = -\left(-\frac{\tilde{u}}{\ell} \right)^{1 - \frac{1}{2n}} e^{2\bar{\mathcal{A}}} d\tilde{u} \, d\hat{v} + (-\tilde{u})^2 R^2 d\theta^2. \quad (41)$$

Rescaling also $\tilde{u}$,

$$\hat{u} = -\ell \left(-\frac{\tilde{u}}{\ell} \right)^{\frac{1}{2n}} \quad \Rightarrow \quad x = \frac{\hat{v}}{\hat{u}}, \quad T = -2n\ln\left(-\frac{\hat{u}}{\ell} \right), \quad (42)$$

the metric becomes

$$ds^2 = -e^{2\hat{\mathcal{A}}} d\hat{u} \, d\hat{v} + \ell^2 \left(-\frac{\hat{u}}{\ell} \right)^{4n} R^2 d\theta^2, \quad (43)$$

where

$$e^{2\hat{\mathcal{A}}} := 4n^2 e^{2\tilde{\mathcal{A}}} \left(\frac{\tilde{u}\tilde{v}}{\ell^2} \right)^{1 - \frac{1}{2n}} = 2n e^{2\bar{\mathcal{A}}} \left(-\frac{\tilde{u}}{\ell} \right)^{2\left(1 - \frac{1}{2n}\right)}. \quad (44)$$

The Garfinkle solution then takes the more symmetric form [16]

$$e^{2\hat{\mathcal{A}}_0} = 4n^2 \left(\frac{\left(-\frac{\hat{u}}{\ell} \right)^n + \left(-\frac{\hat{v}}{\ell} \right)^n}{2} \right)^{4\tilde{c}^2}, \quad (45)$$

$$\bar{r}_0 = \ell \frac{\left(-\frac{\hat{u}}{\ell} \right)^{2n} - \left(-\frac{\hat{v}}{\ell} \right)^{2n}}{2}, \quad (46)$$

$$\phi_0 = -2c\ln\left(\frac{\left(-\frac{\hat{u}}{\ell} \right)^n + \left(-\frac{\hat{v}}{\ell} \right)^n}{2} \right). \quad (47)$$

This is again analytic at both the centre and lightcone (and of course everywhere in between) for $n = 1, 2, \ldots$

B. Continuation beyond the lightcone

As for integer n the Garfinkle metric and scalar field are analytic in x, they can be analytically extended to negative x simply by considering values of x in the range $-1 < x \le 1$.

For both even and odd n, every centred ring in the the region $-1 < x < 0$ is an outer-trapped surface, and $x = -1$ is a future spacelike central curvature singularity (with $M = 1$ at $\bar{r} = 0$), where the Ricci scalar blows up. In this sense, the analytically extended Garfinkle solution could be described as a black hole that is CSS rather than stationary.

Our numerical evidence rules out the analytic continuation, but seems to be compatible with an alternative continuation, where everything depends only on retarded time (assuming that $\Lambda = 0$, as we did in the Garfinkle solution). We shall call this the "null continuation" of the Garfinkle solution, and also denote it by the suffix 0. At $\hat{v} = 0$, the Garfinkle solution (45-47) can be

matched to

$$e^{2\hat{\mathcal{A}}_0} = 4n^2 \left(\frac{\left(-\frac{\hat{u}}{\ell}\right)^n}{2}\right)^{4\tilde{c}^2}, \tag{48}$$

$$\bar{r}_0 = \ell \frac{\left(-\frac{\hat{u}}{\ell}\right)^{2n}}{2}, \tag{49}$$

$$\phi_0 = -2c \ln\left(\frac{\left(-\frac{\hat{u}}{\ell}\right)^n}{2}\right). \tag{50}$$

As the power $\hat{v}^n$ is unmatched, the matching is C^{n-1}. Equivalently, in terms of the similarity coordinates (x, T) and the similarity variables R and $\bar{\mathcal{A}}$, we can match (35-37,39) to

$$e^{2\bar{\mathcal{A}}_0} = 2^{-4\tilde{c}^2}, \tag{51}$$

$$R_0 = \frac{1}{2}, \tag{52}$$

$$\phi_0 = c(T + 2\ln 2), \tag{53}$$

$$M = 0. \tag{54}$$

As the power x^n is unmatched, the matching is again C^{n-1}.

From these two forms of the metric we see that the null continuation has a translation invariance in $\hat{v}$, in addition to circular symmetry and CSS. It can be thought of as an outgoing Vaidya metric. If we think of an event horizon in spherical symmetry as an outgoing null surface of constant area radius $\bar{r}$, then the null continuation is an onion with each layer representing an event horizon, and a null singularity at its centre.

C. The similarity coordinate $\bar{\lambda}(x)$

We can rewrite (29) in generality as

$$s_{,x}(x, T) = -\frac{1}{2}\ell e^{-T + 2\bar{\mathcal{A}}(x,T)}. \tag{55}$$

Hence in the Garfinkle solution, $\lambda := s/(-\tilde{u})$ is given by [11]

$$\lambda_n(x) = n \int_x^1 \left(\frac{1 + x^n}{2}\right)^{4\tilde{c}^2} dx \tag{56}$$

$$= 4^{\frac{1}{n} - 2} n \left[F_1^2 \left(\frac{2}{n} - 4, \frac{1}{n}, \frac{1}{n} + 1, -1\right) \right.$$

$$\left. - x F_1^2(\dots, -x^n) \right]. \tag{57}$$

This is a well-behaved function of x, with $\lambda_4(0) \simeq 0.8377$ and $\lambda_4'(0) \simeq -0.3536$. (Recall the centre is at $x = 1$ and the lightcone at $x = 0$.) For even n, λ is an odd function of x. In our plots we use $\bar{\lambda} := \lambda/\lambda_4(0)$, so that the lightcone of the $n = 4$ Garfinkle solution is at $\bar{\lambda} = 1$, and the analytically extended $n = 4$ Garfinkle solution

is covered by the range $0 \leq \bar{\lambda} < 2$, with f and R even about $\bar{\lambda} = 1$ and M odd. In the null-extended Garfinkle solution $\lambda(x)$ is given by

$$\lambda = \begin{cases} \lambda_n(x), & x > 0 \\ \lambda_n(0) + \lambda_n'(0)x, & x < 0, \end{cases} \tag{58}$$

where we have imposed continuity of s and $s_{,\hat{v}}$ at $\hat{v} = 0$, and hence of λ and $\lambda_{,x}$ at $x = 0$.

D. Boundary conditions and gauge conditions

To fix the residual gauge freedom in double null coordinates, we need two gauge conditions. One of these is always taken to be $\bar{r} = 0$ at $u = v$ in [11, 13, 16], that is, the centre is at $r = 0$, which also corresponds to $x = 1$.

In the Garfinkle solution [11] and in its Λ corrections [16], the second gauge condition is chosen to be $\tilde{\mathcal{A}} = 0$ at $r = 0$. This means that $\tilde{u}$ and $\tilde{v}$ are proper time at the centre.

However, Garfinkle and Gundlach [13] deviate from this last gauge condition for the growing perturbations because in the similarity coordinates (x, T) these can be made regular only for a different gauge choice. (The gauge in which each growing perturbation is regular is linked to the gauge in which $\mathcal{A} = 0$ at $r = 0$ by the infinitesimal gauge transformation generated by the vector field ξ given in (68) below, for a specific value of c_1 chosen to cancel a singularity at $x = 0$.)

With the gauge choice $\bar{r}(0, t) = 0$, the absence of a conical singularity in the metric requires that $\bar{r} = r \exp \mathcal{A} + O(r^3)$, or equivalently $\bar{r}_{,r} = \exp \mathcal{A}$ at $r = 0$. For consistency, this requires also $\phi_{,r} = 0$ and $\mathcal{A}_{,r} = 0$ at $r = 0$. Hence we have three regularity conditions to impose at $x = 1$.

By the definition of x, the lightcone is at $x = 0$, which corresponds to $\tilde{v} = 0$. The solution is analytic there if $\bar{\mathcal{A}}$, $\bar{r}$ or equivalently R, and f are analytic in (x, T) at $x = 0$.

E. Perturbations of the Garfinkle solution

This subsection is based on [13] and is included here for completeness. We slightly rewrite the ansatz of [13] as

$$\tilde{\mathcal{A}} = \tilde{\mathcal{A}}_0(x) + e^{kT}a(x), \tag{59}$$

$$R = R_0(x) + e^{kT}b(x), \tag{60}$$

$$\phi = c[T + f_0(x) + e^{kT}h(x)], \tag{61}$$

where $\tilde{\mathcal{A}}_0$, R_0, f_0 denotes the Garfinkle solution. (The correspondence of notation is $y = x^n$ and $H = ch$, with a and b having the same meaning.)

The regularity conditions on $\tilde{\mathcal{A}}$, R and ϕ are

$$a'(1) + nka(1) = 0, \tag{62}$$

$$b'(1) + n[(k-1)b(1) + a(1)] = 0, \tag{63}$$

$$h'(1) + nkh(1) = 0, \tag{64}$$

and the gauge conditions are

$$b(1) = 0, \tag{65}$$
$$a(1) = 0. \tag{66}$$

Note (66) will be modified below for growing perturbations. The ODEs for b, h and a can be solved in this sequence, and are second-order, second-order and first-order respectively.

The general solution of the ODE for b is

$$b(x) = c_0 + c_1 \left[1 - x^{2n(1-k)} \right], \tag{67}$$

and this is pure gauge. We set $c_0 = 0$ to impose the gauge condition (65) and keep the centre at $x = 1$, but leave c_1 arbitrary. Note that the regularity condition (64) is obeyed for any c_1.

The general infinitesimal gauge transformation that preserves the double null form of the metric in (u, v) is $\xi = f(u)\partial_u + g(v)\partial_v$. Preserving the gauge condition that the centre is at $r = 0$ then requires $f = g$. If we also require the gauge transformation to be compatible with the mode ansatz (59-61), it becomes unique up to an overall factor, which we can choose to be c_1:

$$\xi = -2c_1 \ell^k \left[(-u)^{1-k} \frac{\partial}{\partial u} + (-v)^{1-k} \frac{\partial}{\partial v} \right] \tag{68}$$

$$= -2c_1 e^{kT} \left[\frac{\partial}{\partial T} + \frac{1}{2n} \left(x - x^{1-2nk} \right) \frac{\partial}{\partial x} \right]. \tag{69}$$

Hence c_1 is also pure gauge, and the remaining gauge freedom in the mode ansatz is parameterised precisely by c_1.

The general solution $h(x)$ that is regular at the centre $x = 1$ is

$$h(x) = c_2 F_a(1 - x^{2n}) - 2c_1 \frac{1 + x^{n(1-2k)}}{1 + x^n}, \tag{70}$$

where $F_a(z)$ stands for a hypergeometric function that is analytic in z for $|z| < 1$ with $F_a(0) = 1$. Hence c_2 multiplies a regular solution of the homogeneous ODE for $h(x)$. The other linearly independent homogeneous solution contains a $\ln(1 - x)$ term, which is singular at the centre, and is therefore ruled out.

Not only for $b(x)$ and $h(x)$ here, but also for $a(x)$ below, all terms proportional to c_1 arise as gauge transformations generated by the vector field ξ defined in (68), and all other terms are proportional to c_2. In this sense any perturbation with $c_2 = 0$ is pure gauge.

For the special case $k = 1$,

$$h(x) = (c_2 - 2c_1) \frac{1 + x^{-n}}{1 + x^n}. \tag{71}$$

Hence the term parameterised by c_2 is also pure gauge. In this case, $\xi = -2c_1 \ell(\partial/\partial t)$, representing just a time translation of the Garfinkle solution. This $k = 1$ time translation mode arises in the perturbation spectrum of any self-similar solution of the Einstein equations.

The special case $k = 0$ corresponds to an infinitesimal perturbation that takes a CSS solution into a neighbouring one. As we have seen that the Garfinkle solution is locally unique once the gauge has been fixed and analyticity imposed at the centre and lightcone, the $k = 0$ perturbations must be pure gauge, and we need not consider them explicitly.

For the special case $k = 1/2$,

$$h(x) = c_2(\text{singular}) - 2c_1 \frac{2}{1 + x^n}. \tag{72}$$

This is singular for any c_1, unless $c_2 = 0$, and so is again pure gauge.

The homogeneous part of $h(x)$ can be written in the form

$$F_a(1 - x^{2n}) = C_b F_b(x^{2n}) + C_c x^{n(1-2k)} F_c(x^{2n}), \tag{73}$$

using formula 15.3.6 of [17]. Here,

$$C_b := \frac{\Gamma\left(\frac{1}{2} - k\right)}{\sqrt{\pi}\Gamma(1 - k)}, \quad C_c := \frac{\Gamma\left(k - \frac{1}{2}\right)}{\sqrt{\pi}\Gamma(k)}. \tag{74}$$

However, this does not hold when $k = \mathbb{Z} + 1/2$. Then either C_b or C_c is formally infinite, and in fact is replaced by a $\ln x$ term. Both hypergeometric functions are by definition regular at $x = 0$. For $k \neq \mathbb{Z} + 1/2$, a necessary condition for the $x^{n(1-2k)}$ term, and hence F_a to be regular at $x = 0$ is that $k = m/2n$ for m integer. From considering the three special cases above, we already have $m \neq 0, n, 2n$.

Setting $k = m/2n$ from now on, we have

$$h(x) = c_2 C_b F_b(x^{2n}) + c_2 C_c x^{n-m} F_c(x^{2n})$$
$$- 2c_1 \frac{1 + x^{n-m}}{1 + x^n}. \tag{75}$$

Hence this is a series in x^n (or in x^{2n} for $c_1 = 1$), plus x^{n-m} times another such series. For $m < n$, every term is regular separately. For $n < m < 2n$, there is precisely one singular power, x^{n-m}, which can be cancelled by setting

$$c_1 = c_2 \frac{C_c}{2}. \tag{76}$$

For $m > 2n$, there is at least a second singular power, which cannot be cancelled, so this must be ruled out (and $m = 2n$ was already ruled out).

Further restrictions on m arise from regularity of $a(x)$ at the lightcone. $a(x)$ takes the form

$$a(x) = 2c_1(1 - k) + \int_1^x a'(x) \, dx, \tag{77}$$

where $a'(x)$ is known in terms of $b(x)$ and $h(x)$ and $a(1)$ is determined by (62). To check regularity at $x = 0$, it is sufficient to check regularity of $xa'(x)$ as $x \to 0$ by expanding it in powers of x. With $k = m/(2n)$, these powers are all integers, so we only need to look for negative powers.

We find that $xa'(x)$ is a regular series in x^n, plus x^{-m} times a regular series in x^n.

Consider first $0 < m < n$. Then the only singular power is x^{-m} and it can be cancelled by choosing

$$2c_1 = \frac{(m-2n)(2n-1)}{m(m-1)} c_2 C_c. \qquad (78)$$

However, in the case $m = 1$ this regularity condition gives $c_2 = 0$ and hence this regular perturbation is pure gauge.

For $n < m < 2n$, the power x^{n-m} is also singular. It is cancelled by the same condition (76) that is already required to make h regular for this range of m. Hence we now have two regularity conditions on c_1, (76) and (78). They are compatible for precisely $m = 2n - 1$.

Hence, from regularity of a at $x = 0$ we have found the additional restrictions that either $m = 2n - 1$ or $m < n$ with $m \neq 0, 1$.

We now summarise the union of all regularity conditions: For a given integer $n > 0$, the perturbation spectrum is given by $k = m/(2n)$ where either $m = 2n - 1$, or $1 < m < n$, or $m < 0$ with $m \neq n(1 - 2\mathbb{N})$. In particular there are $n - 1$ growing perturbations given by $m = 2, 3, \ldots, n - 1$ and $m = 2n - 1$.

F. Perturbations of the null continuation

The linear perturbations of the null continuation, with $k = m/(2n)$ are

$$b(x) = (d_0 + d_1) + d_2 x, \qquad (79)$$

$$h(x) = -2(d_0 + d_1) + d_4 - \frac{2nd_2}{1 + m - n} x + d_3 x^{n-m}, \quad (80)$$

$$\begin{aligned}
a(x) = &-\frac{(1 + m - 4n)(d_0 + d_1) + (2n - 4)d_4}{2n} \\
&+ \frac{n(2n-1)d_2}{(1+m)(1+m-n)} x + \frac{(1-m)d_1 + 2nd_5}{2n} x^{-m} \\
&+ \frac{(1-2n)d_3}{2n} x^{n-m},
\end{aligned} \qquad (81)$$

subject to the condition that either $m = 2n-1$ or $d_2 = 0$. Hence this is a 5-parameter family of solutions for generic m, or 6-parameter in the particular case $m = 2n-1$. The parameterisation has been chosen such that the solution with $d_0 = c_0$, $d_1 = c_1$ and $d_2 = d_3 = d_4 = d_5 = 0$ is pure gauge, generated by the vector field ξ. (We have not yet set $c_0 = 0$ here, as the reason for doing so for perturbations of the Garfinkle solutions was only to fix the centre at $x = 1$.)

G. Matching of perturbations on the lightcone

For $m < 0$, when c_1 and c_2 can be chosen independently, the perturbations b and h of the Garfinkle solution take the following values on the lightcone $x = 0$:

$$b(0) = c_1, \qquad (82)$$
$$h(0) = -2c_1 + c_2 C_c. \qquad (83)$$

For the allowed values of $m > 0$, where c_1 is linked to c_2 for regularity at the lightcone, they take the equivalent values with c_1 given by (78). The value of $a(0)$ can then be obtained from the linearisation of the $\bar{r}_{,uu}$ field equation (14), which at $x = 0$ reduces to the algebraic equation

$$a(0) + \left(k - \frac{1}{2n}\right) b(0) + \left(1 - \frac{1}{2n}\right) h(0) = 0. \qquad (84)$$

In matching to the perturbations of the null continuation, continuity of b and h at $x = 0$ is required by physical regularity of the spacetime (absence of a thin shell of matter at the matching surface). This fixes

$$d_1 = c_1 - d_0, \qquad (85)$$
$$d_4 = c_2 C_b. \qquad (86)$$

Continuity of a follows because (84) holds on both sides.

We can use the remaining free parameters d_i to make the metric in coordinats (x, T) more differentiable at $x = 0$ by matching the lowest non-zero powers of x. We begin with the case $m < 0$, which implies $d_2 = 0$ and allows c_2 and c_1 to be chosen independently. We set

$$d_3 = -2c_1 + c_2 C_c. \qquad (87)$$

in order to match the coefficients of x^{n-m} in $h(x)$ on both sides. The same choice of d_3 matches the coefficient of x^{n-m} in $a(x)$, and we can match the coefficient of x^{-m} in $a(x)$ as well by setting

$$d_5 = \frac{1 - 2kn}{2n} d_0 + c_2 C_c \frac{(2k-1)(2n-1)}{4kn}. \qquad (88)$$

Although we have not formally determined d_0, it cancels out of the resulting expressions for $b(x)$, $h(x)$ and $a(x)$, so that we have specified a unique maximally differentiable continuation, in the sense that the coefficients of all powers of x on the outer side match those of the expansion in x on the inner side, and all unmatched powers are higher.

The case $1 < m < n$ is obtained from the case $m < 0$ by imposing the particular gauge choice (78). In particular, the coefficients of the singular power x^{-m} in $a(x)$ then vanishes on both sides.

In the special case $m = 2n - 1$, we have the additional parameter d_2 on the outer side. We set the other parameters as before, and $d_2 = -c_1$. b, h and a in the outer region are now all linear functions of x. Once again, this choice is maximally differentiable in the sense above. (For b, it happens to be analytic, as the expressions for $b(x)$ on both sides coincide.)

Expressing the perturbations of the null continuation in terms of the free parameters c_1 and c_2 only, we have,

for $m < 0$,

$$b(x) = c_1, \tag{89}$$

$$h(x) = (c_2 C_b - 2c_1) + (c_2 C_c - 2c_1)x^{n-m}, \tag{90}$$

$$a(x) = -\frac{c_2 C_b(2n-1) + c_1(m+1-4n)}{2n}$$
$$+ \frac{c_2 C_c(m-n)(2n-1) - m(m-1)c_1}{2mn}x^{-m}$$
$$+ - \frac{(c_2 C_c - 2c_1)(2n-1)}{2n}x^{n-m}. \tag{91}$$

The case $1 < m < n$ is obtained from the case $m < 0$ by imposing the particular gauge choice (78). The case $m = 2n - 1$ is given by

$$b(x) = c_2 \frac{C_c}{2}(1-x), \tag{92}$$

$$h(x) = c_2\left[(C_b - C_c) + C_c x\right], \tag{93}$$

$$a(x) = c_2\left[\frac{C_b(1-n) + C_c n}{2n} + \frac{C_c(1-2n)}{4n}x\right]. \tag{94}$$

H. Λ corrections of the Garfinkle solution

This subsection is based on [16], and is included here for completeness. If the field equations are not scale-invariant but scale-invariance holds asymptotically on sufficiently small scales, the critical solution itself may be approximated by an expansion in powers of (typical length scale of the solution)/(length scale set by the field equations). This was discussed in generality in [18], where it was also shown formally that the leading order of this expansion represents a scale-invariant solution, and that the perturbation spectrum is given by the perturbation spectrum of that leading order. In our current problem, the only length scale in the field equations is ℓ defined by $\Lambda = -\ell^{-2}$, and so the required expansion is one in powers of $\exp(-T) = -\tilde{u}/\ell$.

The leading order of this expansion about the Garfinkle solution was given in [16]. We slightly rewrite their ansatz as

$$\tilde{\mathcal{A}} = \tilde{\mathcal{A}}_0(x) + \sum_{n=1}^{\infty} e^{-2nT} \mathcal{A}_n(x), \tag{95}$$

$$R = R_0(x) + \sum_{n=1}^{\infty} e^{-2nT} R_n(x), \tag{96}$$

$$\phi = c\left[T + f_0(x) + \sum_{n=1}^{\infty} e^{-2nT} f_n(x)\right] \tag{97}$$

(The correspondence of notation is $\mathcal{A}_1$, $R_1 = F$, $f_1 = H/c$, $y = x^n$ as before, and their c is our $\tilde{c}$, with their u and v our $\hat{u}$ and $\hat{v}$.)

The field equations give five ODEs for R_1, f_1 and $\mathcal{A}_1$, equivalent to the $k = -2$ perturbation equations but with source terms proportional to Λ. We only need to obtain a particular integral. The general solution is then obtained by adding the homogenous $k = -2$ perturbations b, h

and a to R_1, f_1 and $\mathcal{A}_1$. The regularity conditions to first order in Λ are

$$\mathcal{A}_1'(1) - 2n\mathcal{A}_1(1) = 0, \tag{98}$$

$$R_1'(1) + n[-3R_1(1) + \mathcal{A}_1(1)] = 0, \tag{99}$$

$$f_1'(1) - 2nf_1(1) = 0, \tag{100}$$

and the gauge conditions are

$$R_1(1) = 0, \tag{101}$$

$$\mathcal{A}_1(1) = 0. \tag{102}$$

These are equivalent to the regularity and gauge conditions for $k = -2$ linear perturbations.

Like b, R_1 obeys a linear second-order ODE that can be solved on its own. The two linearly independent homogeneous solutions are known in closed form and are 1 and x^{6n}, compare (67). This can be used to write a particular solution in the form of an integral using variation of parameters. Alternatively, [16] use the fact that R_1 does not appear undifferentiated to first solve for R_1' using an integrating factor.

With $R_1(x)$ determined, f_1 obeys a linear second-order ODE that can be solved on its own. Again the homogeneous solution is known, and so a particular integral can be given as an integral using variation of parameters [16].

The remaining three ODEs, which are of course consistent with each either because of the Bianchi identities, can be reduced to obtain an algebraic expression for $\mathcal{A}_1 = \mathcal{A}_1(R_1', R_1, f_1', f_1, x)$. As for the linear perturbations, the first Λ correction of the $\bar{r}_{,uu}$ field equation becomes an algebraic constraint on the lightcone, namely

$$2n\mathcal{A}_1(0) + (2n-1)f_1(0) - (4n+1)R_1(0) = 0. \tag{103}$$

Either of the integral expressions for R_1 gives rise to a messy expression in terms of hypergeometric functions, and we have not been able to evaluate any integral expression for $\mathcal{A}_1$ in closed form. Hence these formal solutions are not very useful for plotting or numerical time evolution. Instead, we obtain a numerical solution by solving the second order ODEs for R_1 and f_1 with the boundary conditions $R_1'(1) = R_1(1) = 0$ and $f_1'(1) = f_1(1) = 0$, respectively. We then solve the $\mathcal{A}_{,uv}$ field equation as a second-order ODE for $\mathcal{A}_1$ with the boundary conditions $\mathcal{A}_1'(1) = \mathcal{A}_1(1) = 0$. (This is numerically more robust than trying to use the algebraic expression or first order ODE for $\mathcal{A}_1$). We add a $k = -2$ linear perturbation with c_1 and c_2 chosen to set $R_1(0) = f_1(0) = \mathcal{A}_1(0) = 0$.
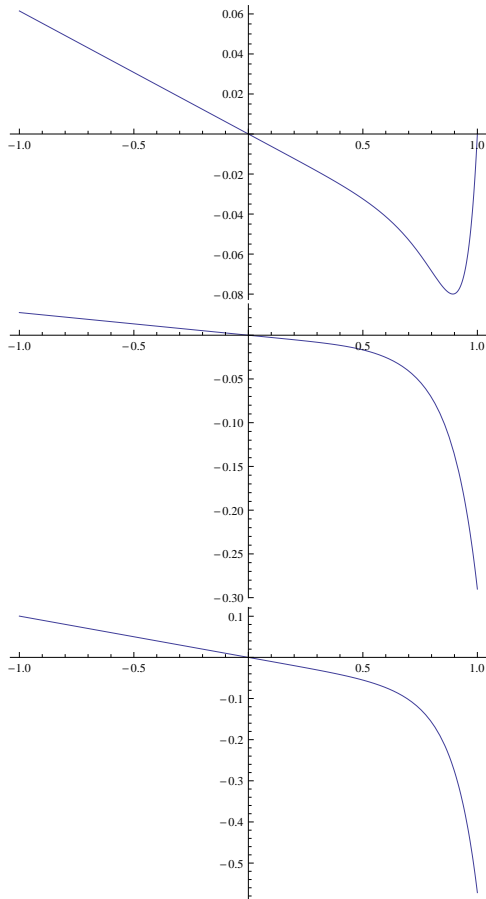
FIG. 31. $R_1(x)$, $f_1(x)$ and $\mathcal{A}_1(x)$ (from top to bottom) against x for $-1 < x < 1$. Note that the regular centre is at $x = 1$ and the lightcone at $x = 0$. In the outer region $x < 0$, these are just the linear functions (104) to (106).

I. Λ corrections of the null continuation

The Λ corrections of the null continuation are given by

$$R_1(x) = \frac{4^{\frac{1}{n}} n^2}{16(1 - 6n)} x, \tag{104}$$

$$f_1(x) = -\frac{4^{\frac{1}{n}} n^3}{8(1 - 5n)(1 - 6n)} x, \tag{105}$$

$$\mathcal{A}_1(x) = \frac{4^{\frac{1}{n}} n^2 (1 - 8n)}{16(1 - 5n)(1 - 6n)} x, \tag{106}$$

This is matched to the highest possible order to the particular Λ correction of the Garfinkle solution specified above. The Λ corrections of the Garfinkle solution with the null continuation, in the gauge where they all vanish at $x = 0$, are shown in Fig. 31.

J. Derivation of γ

We conjecture that for a yet unknown reason the true critical solution has only one growing mode with Lya-

punov exponent λ_0. Then the scaling of the maxima and minima of Ricci and their location in proper time (relative to the accumulation point and relative to each other) can be calculated by the standard argument based on dimensional analysis [2, 3]. We summarise it here for completeness.

Assume that the first maximum of Ricci is reached when the solution moves away from the critical solution, and that this happens when the one growing mode has reached some $O(1)$ reference amplitude at which the growing perturbation becomes nonlinear and stops growing exponentially in T. This gives

$$|p - p_*| e^{\lambda_0 T_{\text{nonlin}}} \propto c_{2,\text{top}} e^{\lambda_0 T_{\text{nonlin}}} \sim 1. \tag{107}$$

Then, because all scales are proportional to $\exp(-T)$ and because the Ricci scalar has dimension of inverse length squared,

$$R_{\text{max}} \propto e^{2T_{\text{nonlin}}} \propto |p - p_*|^{-2\gamma}, \tag{108}$$

where

$$\gamma = \frac{1}{\lambda_0} = \frac{2n}{2n - 1} = \frac{8}{7} \simeq 1.1429, \tag{109}$$

and we have assumed $n = 4$ in the last equality. After the growing mode has become nonlinear, the evolution is no longer CSS, but as we are now on very small scales, the cosmological constant can locally be neglected with respect to the scalar field gradient (squared) in the stress-energy tensor. Hence the subsequent local evolution is approximately scale-invariant, and its actual overall length scale is set by the length scale of the interim data at T_{nonlin}, which is $\ell \exp T_{\text{nonlin}}$. We have found numerically that this universal subsequent evolution has (at least) two maxima and two minima before blowup. As the entire solution scales, so will both the locations in proper time of these extrema (as $|p - p_*|^\gamma$), and their values.

K. Derivation of δ

The "standard" argument [2, 3] would now continue by noting that in near-supercritical evolutions the above-mentioned universal evolution results in a black hole, and that the linear size of this black hole scales with the overall length scale, and hence as $|p - p_*|^\gamma$. In $d + 1$ spacetime dimensions, the black hole mass has units of $(\text{length})^{d-2}$, and so scales as $|p - p_*|^\delta$ with $\delta = (d - 2)\gamma$. However, in $d = 2$ this argument fails because M is dimensionless. We also know that no black holes can form from regular data for $\Lambda = 0$, and so it is clear that Λ must play a role, leading to anomalous scaling exponent. The following theoretical model appears to be consistent with our numerical experiments.

Assume that the true critical solution is well approximated by the $n = 4$ Garfinkle solution inside the lightcone and its null continuation outside the lightcone, plus

their first Λ corrections. (For clarity of presentation only, we retain the generic n.) Assume further that the true critical solution has only one growing mode that is well approximated by the $m = 7$ (top) perturbation mode, while the $m = 2, 3$ modes disappear in the true critical solution.

By definition, a MOTS is given by $\bar{r}_{,\hat{v}} = 0$, meaning that the area radius does not grow on an outgoing null ray. (We use $\bar{r}_{,\hat{v}}$ because $\hat{v}$ is a regular coordinate at the lightcone while $\tilde{v}$ is not.) In terms of $R(x, T)$, this is given by

$$\bar{r}_{,\hat{v}}(\hat{u}, \hat{v}) = -e^{\left(\frac{1}{2n} - 1\right)T} R_{,x}(x, T). \qquad (110)$$

In the null-continued Garfinkle solution without any Λ corrections, every point in the (r, t) plane outside the lightcone is a MOTS, and so the AH is not well defined. Therefore we add the first-order Λ corrections. From Fig. 31 we see that everywhere except close to the centre $R_1'(x) < 0$ and so this will make $R_{,x}$ more negative. But close to the centre where $R_1'(x) > 0$, $|R_0'(x)| \gg \exp(-2T)|R_1'(x)|$, and so $R_{,x}$ remains negative there, too. Outside the lightcone, $R_0'(x) = 0$ and $R_1'(x) < 0$, so $R_{,x}$ is also negative. Hence the leading Λ correction removes all MOTS, as already pointed out for the Garfinkle solution (inside the lightcone) in [16].

Assuming that we have fine-tuned the initial data and have reached large T, we now add the growing perturbation mode, but neglect all decaying modes. Given that the Λ corrections have removed MOTS already in perturbation theory, we shall see that the growing perturbation mode will bring them back for $p > p_*$. We begin with the region outside the lightcone, where

$$R_{,x}(x, T) = e^{-2T} R_1'(x) + c_{2,\text{top}} e^{\lambda_0 T} b_{\text{top}}'(x) \qquad (111)$$

$$= e^{-2T} \frac{4^{\frac{1}{n}} n^2}{16(1 - 6n)} - c_{2,\text{top}} e^{\lambda_0 T} \frac{C_{c,\text{top}}}{2} (112)$$

Here "top" denotes the most rapidly growing mode, with $m = 2n - 1$, and hence $\lambda_0 = 1 - \frac{1}{2n}$. We have assumed that the other growing modes, with $1 < m < n$, of the null-continued Garfinkle solution are not present in the true critical solution. [However, from (79) we see that $b'(x) = 0$ for these modes, so they would not contribute to $R_{,x}(x, T)$ anyway.] Recall also that $R_0'(x) = 0$ in the outer region, and so does not contribute to $\bar{r}_{,\hat{v}}$.

If there is only one growing mode, then its amplitude must be zero at $p = p_*$, and so must be proportional to $p - p_*$ to leading order. Hence, outside the lightcone, an AH is present for $c_2 > 0$, corresponding by assumption to $p - p_* > 0$. It is the outgoing null surface $T = T_{\text{AH},0}$, given by

$$\bar{r}_{,\hat{v}} = 0 \quad \Leftrightarrow \quad p - p_* \propto c_{2,\text{top}} \propto e^{-(2+\lambda_0)T_{\text{AH},0}}, \quad (113)$$

where the proportionality signs hide irrelevant constant factors. But on this null segment of the AH,

$$M_{\text{AH},0} = \frac{\bar{r}^2}{\ell^2} = R^2 e^{-2T} = \frac{1}{4} e^{-2T_{\text{AH},0}} \propto (p - p_*)^\delta, \quad (114)$$

where

$$\delta = \frac{2}{2 + \lambda_0} = \frac{4n}{6n - 1} = \frac{16}{23} \simeq 0.6957, \qquad (115)$$

and we have assumed $n = 4$ in the last equality. Note this is the mass on the null part of the AH outside the lightcone, not yet the mass of the EMOTS. However, inside the lightcone the contribution of $R_0'(x)$ to $R_{,x}(x, T)$ dominates the contributions of the Λ correction and the perturbation modes except just inside the lightcone, where $R_0'(x) \to 0$ as $x \to 0_+$. We conclude without explicit calculation that the AH must continue as a (probably spacelike) surface running just inside the lightcone. Hence the EMOTS, or minimum of $t_{AH}(r)$, must occur just inside the lightcone of the critical solution. Hence

$$M_{\text{EMOTS}} \simeq M_{\text{AH},0}. \qquad (116)$$

Moreover, while the EMOTS is slicing-dependent, the theoretical AH curve $\bar{r}_{,\hat{v}} = 0$ plotted in the regular coordinates $(\hat{u}, \hat{v})$ makes a sharp bend from "almost" ingoing null to outgoing null as it crosses the lightcone. This shape is confirmed by plots of the AH in coordinates (t, r) in near-critical numerical evolutions. Hence almost any time slice will first intersect the AH at this sharp bend, and so the location of the EMOTS and its mass depend only weakly on the slicing.

Numerical data confirm that the EMOTS occurs just inside the lightcone, or

$$\tilde{u}_{\text{EMOTS}} \ll \tilde{v}_{\text{EMOTS}} < 0, \qquad (117)$$

For sub8 to sub20 Gaussian data, $\tilde{v}_{\text{EMOTS}}/\tilde{u}_{\text{EMOTS}} \propto (p - p_*)^{0.7}$. For sub20 to sub26 data, $\tilde{v}_{\text{EMOTS}}$ is approximately constant. The numerical data also confirm that

$$M_{\text{EMOTS}} \simeq \frac{1}{4} \left(-\frac{\tilde{u}_{\text{EMOTS}}}{\ell} \right)^2. \qquad (118)$$

Consider now the very special initial data consisting of the critical solution plus a small amplitude p times the growing mode. For sufficiently large (but still very small) p, such that $T = T_{\text{AH},0}$ intersects the initial data surface $t = 0$, we expect a MOTS to be present in the initial data. More precisely, if we evolved these initial data backwards in time we would find that the EMOTS had formed at some $t < 0$, roughly where $T = T_{\text{AH},0}$ intersects the lightcone of the critical solution. We have argued above that the AH extends from the EMOTS towards larger r as the curve $T = T_{\text{AH},0}$ with constant mass. Hence the MOTS at the intersection of $t = 0$ with the AH still has the same mass as the EMOTS did.

The value of $\delta = 16/23$ derived here compares well with our numerical value of $\delta \simeq 0.68(4)$, but we cannot be sure that $\lambda_0 = 7/8$ exactly in the true critical solution. Hence we note that, with $\gamma = 1/\lambda_0$, (115) can be restated more robustly as

$$\delta = \frac{2\gamma}{2\gamma + 1}, \qquad (119)$$

independently of the value of γ. What has gone into this relation is the assumption that both the Λ correction and the growing mode make a constant contribution to $R_{,x}$ at leading order – something we would expect to hold to leading order in x for smooth functions.

L. An exact continuation of the Garfinkle solution beyond the lightcone with $\Lambda < 0$

Three clear observations in near-critical evolutions of generic initial data were that the critical solution outside the lightcone appears to have $M \simeq 0$, $R \simeq 1/2$ and $\phi \simeq cT$. As we have seen, these are exact properties of the null continuation, but the null continuation is a solution only for $\Lambda = 0$. This can be rectified by incorporating the effects of Λ perturbatively, as we have done in Sec. III I. However, an *exact* solution can also be found in which these qualitative features hold, and which perturbatively reduces to the null continuation with Λ corrections.

Consider again the metric (31). For general $\bar{\mathcal{A}}(x,T)$ and $R(x,T)$, with the scalar field $\phi = c[T + f(x,T)]$, this ansatz is generic, with $T = \text{const}$ and $x = 0$ null by ansatz. As we saw, for $\bar{\mathcal{A}} = \bar{\mathcal{A}}(x)$ and $R = R(x)$, compatible with $f = f(x)$, the metric is CSS. Consider now instead

$$\bar{\mathcal{A}} = \check{\mathcal{A}}(\check{x}), \tag{120}$$

$$R = \check{R}(\check{x}), \tag{121}$$

$$f = \check{f}(\check{x}), \tag{122}$$

where we have defined the "slow x"

$$\check{x} := e^{-2T} x. \tag{123}$$

Note the lightcone is at $x = \check{x} = 0$.

To understand the geometric significance of this ansatz, we express the metric (31) with (120-122) in the coordinates $(\check{x}, T)$ instead of (x, T). The result is

$$ds^2 = \ell^2 \left[e^{2\check{\mathcal{A}}} \left(d\check{x} - \frac{\check{x}}{2\check{n}} \, dT \right) dT + e^{-2T} \check{R}^2 \, d\theta^2 \right], \tag{124}$$

where we have defined the constant

$$\check{n} := \frac{n}{1 - 4n}. \tag{125}$$

The functional form of this metric differs from (31) only by the absence of the overall factor $\exp(-2T)$ in the metric in the (x, T) plane. Hence, $K := \partial/\partial T$ now acts as a homothetic vector field only on the metric along the orbits of the circular symmetry, but as a Killing vector field on its orthogonal complement. We can also see immediately that the mass function (17) now takes the form

$$M = \mu(\check{x})e^{-2T}, \tag{126}$$

and so is exponentially small.

It is straightforward to verify that the ansatz (120-122) transforms the five field equations *exactly* into ODEs in $\check{x}$. Moreover, by introducing the auxiliary variables

$$\check{F}(x) := \check{f}'(\check{x}), \qquad \check{\rho}(\check{x}) := \frac{\check{R}'(\check{x})}{\check{R}(\check{x})}, \tag{127}$$

we reduce this system to the pair of first-order ODEs

$$\check{F}' = \frac{(\check{n} - 1 - \check{x}\check{\rho})\check{F} - \check{n}\check{\rho}}{\check{x}}, \tag{128}$$

$$\check{\rho}' = \frac{-\tilde{c}^2 \check{x}(\check{F}^2 + 2\check{\rho}\check{F}) + \check{\rho}[\check{x}\check{\rho} - 2\check{n}(1 + \tilde{c}^2) - 1]}{\check{x}}, \tag{129}$$

and the constraint

$$e^{2\check{\mathcal{A}}} = \frac{\tilde{c}^2 \check{x}(\check{F}^2 + 2\check{\rho}\check{F}) - \check{\rho}[2\check{x}\check{\rho} - 2\check{n}(2 + \tilde{c}^2)]}{\check{n}}. \tag{130}$$

Here the constant $\tilde{c}$ is related to the constant c by (33), and hence to the constant n by (38).

Consider for a moment the parameter $\check{n}$ as unrelated to n. Locally in $\check{x}$, the reduced system then has a 2-parameter family of solutions. The solution $(\check{\mathcal{A}}, \check{R}, \check{f})$ follows by integration, where an additive constant in $\check{f}$ and a constant factor in $\check{R}$ can be fixed arbitrarily. Moreover, the system has a scale invariance that reflects an arbitrary overall factor in the definition of $\check{x}$, for a third integration constant.

If we want the solution to include a regular lightcone $\check{x} = 0$, we we are forced to choose

$$\check{n} = -\frac{1}{2(1 + \tilde{c}^2)}. \tag{131}$$

Modulo (38), this is equivalent to (125). The solution with a regular lightcone is then unique, up to the above-mentioned three integration constants. $\check{\rho}(x) > 0$ throughout this solution, meaning that there are no outer-trapped surfaces.

Choosing furthermore $n = 4$, the equations become

$$\check{F}' = \frac{4\check{\rho} - \check{F}(19 + 15\check{x}\check{\rho})}{15\check{x}}, \tag{132}$$

$$\check{\rho}' = -\frac{7\check{F}^2}{8} - \frac{7\check{F}\check{\rho}}{4} + \check{\rho}^2, \tag{133}$$

$$e^{2\check{\mathcal{A}}} = \frac{-105\check{x}\check{F}^2 - 210\check{x}\check{F}\check{\rho} + 8\check{\rho}(23 + 30\check{x}\check{\rho})}{32}. \tag{134}$$

We can use the three integration constants to match the regular light cone solution to the Garfinkle solution at the lightcone continuously (but of course not analytically). In particular, $\check{\rho}(0)$ fixes the overall scale of $\check{x}$.

To compare our numerical solutions against this exact solution, we note that, from (55), we have

$$s_{,\check{x}}(\check{x}, T) = -\frac{1}{2}\ell e^{T + 2\check{\mathcal{A}}(\check{x})}, \tag{135}$$

and we can use this to define $\check{x}$ from the affine parameter s along outgoing null curves, with $s = 0$ on the lightcone

of the critical solution, so that $s(\check{x} = 0) = 0$. Hence to check for this symmetry, we should plot $\bar{\mathcal{A}}$, R and f against the similarity coordinate

$$\check{\lambda} := \frac{s - s_{\text{lightcone}}}{\ell e^T} = e^{-2T}(\bar{\lambda} - 1), \qquad (136)$$

We compute $\check{\lambda}$ in the exact solution as

$$\check{\lambda} = -\frac{1}{2} \int_0^{\check{x}} e^{2\check{\mathcal{A}}(\check{x})} \, d\check{x}. \qquad (137)$$

The regular lightcone solution blows up at $\check{x} \simeq 40$ (inside the lightcone) with $R \to 0$, meaning that in this ansatz we cannot have both a regular lightcone and a regular centre. This is not surprising, and we do not want to use this ansatz inside the lightcone anyway. It also blows up at $\check{x} \simeq -10$ (outside the lightcone) with $R \to \infty$ and $s \to \infty$, so this blowup is likely to be caused only by infinity being mapped to a finite coordinate value.

Taylor-expanding about $\check{x} = 0$, we obtain

$$\check{R}(\check{x}) = \check{R}(0) + \frac{d\check{R}}{d\check{x}}(0) \, \check{x} + O(\check{x}^2)$$

$$= \check{R}(0) + \frac{d\check{R}}{d\check{x}}(0) \, e^{-2T} x + O\left(e^{-4T} x^2\right)$$

$$= R_0(0) + e^{-2T} \frac{dR_1}{dx}(0) \, x + \dots$$

$$= R_0(x) + e^{-2T} R_1(x) + \dots \qquad (138)$$

[The third equality follows from matching, and the last equality because $R_0(x)$ is constant and $R_1(x)$ proportional to x.] Hence to this order we recover the null continuation and its first Λ correction. We expect that higher orders in $\check{x}$ correspond to higher Λ corrections (fixing a suitable gauge at each order in $\exp{-2T}$).

In our numerical simulations, we only access very small (negative) values of $\check{x}$ and hence $\check{\lambda}$, because $\exp(-2T)$ is small. This means that we cannot distinguish the exact solution from its approximation to first order in Λ. In fact, other deviations from the null continuation (the zeroth order) from other sources are already larger than the first Λ correction.

It is possible that there exists an analytic function $\xi(x, T)$ such that $\xi \simeq x$ for $1 > x > \epsilon$ and $\xi \simeq \check{x}$ for $x < -\epsilon$, with a transition in a boundary layer of width ϵ around the lightcone, and such that making $\bar{\mathcal{A}}$, R and f functions of $\xi(x, T)$ only transforms the field equations into ODEs in ξ. However, if there is no ξ that gives rise to a global ODE system then it may still be possible to make a simple ad-hoc ansatz for ξ, and expand the corresponding PDE system in powers of $\exp(-2T)$ on both sides of the lightcone at once, rather than separately, as we have done, thus maintaining analyticity at the lightcone order by order in Λ.

M. Construction of initial data for the amended Garfinkle solution

To extract the free initial data $B(r)$, $B_{,t}(r)$, $\phi(r)$, $\phi_{,t}(r)$ for the Cauchy code based on (19), we need to define a time slice $t = 0$ through that solution, and a radial coordinate r on it, such that both are regular, and $t \pm r$ are null coordinates. We choose $t = (\hat{v} + \hat{u})/2 + \text{const.}$ and $r = (\hat{v} - \hat{u})/2$, where $\hat{u}$ and $\hat{v}$ in turn are related to x and T by (42).

The Garfinkle solution assumes $\Lambda = 0$ whereas the form (19) of the metric has an inbuilt compactification at timelike infinity that makes sense only if $\Lambda < 0$. We therefore make a smooth switchover from the initial data discussed above in an interior region, to vacuum data $\phi_{,r} = \phi_{,t} = 0$ in the gauge $B_{,r} = B_{,t} = 0$ in an exterior region. We then solve the constraint equations (8) and (9) of [9] as algebraic equations for $A_{,t}(r, 0)$ and $A_{,r}(r, 0)$, and then solve a first-order quasilinear ODE for $A(r, 0)$. This pair of algebraic equations becomes singular on MOTS, and so we must include the first Λ corrections in the data to avoid MOTS. For the same reason, we do not try to impose the gauge $B(r, 0) = B_{,t}(r, 0) = 0$ that we have used for evolving generic initial data.

The resulting initial data are parameterised by T_{initial}, the value of T at $(r = 0, t = 0)$, which governs the magnitude of the Λ corrections, the value $r_{\text{lightcone}}$ of r where the lightcone of the Garfinkle solution intersects $t = 0$, and the location r_0 and width Δr of the switchover from Garfinkle to trivial data. The switched initial data are obtained by multiplying the initial data for $B_{,r}$, $B_{,t}$, $\phi_{,r}$ and $\phi_{,t}$ by a switch-off function $\chi_-(r)$ that goes smoothly to zero, then integrating to get initial data for B and ϕ, and finally solving the constraints to get initial data for A and $A_{,t}$.

We use the switch-off function χ_- defined by

$$\chi_-(r) := \frac{1 - \chi\left(\frac{r - r_0}{\Delta r}\right)}{2}, \qquad (139)$$

$$\chi(x) := \tanh\left[18\left(\frac{1}{4}x + \frac{3}{4}x^3\right)\right]. \qquad (140)$$

The coefficients of x and x^3 in $\chi(x)$ have been chosen so that when we work in double precision the switching happens effectively between $r_0 - \Delta r$ and $r_0 + \Delta_r$, while at the same time minimising the first four derivatives of $\chi(x)$.

IV. CONCLUSIONS

The presence of a negative cosmological constant in massless scalar field collapse adds reflecting boundary conditions and breaks scale invariance. However, simulations in 3+1 and higher dimensions have shown that there is a regime in phase space where the outer boundary conditions are irrelevant and the local dynamical effect of the cosmological constant is neglible compared to the scalar

field stress-energy tensor. Critical collapse then proceeds as without a cosmological constant, showing local discrete self-similarity and scaling of the maximal curvature (for subcritical data) or initial black hole mass (for supercritical data). (The word "initial" had to be inserted here as the reflecting boundary conditions will lead to continuing growth of the black hole mass.)

In 2+1 dimensions significant differences are clear a priori: Energy and mass are dimensionless, and hence the dimensional analysis formula (3) linking Ricci and black hole mass scaling cannot hold. There is a mass gap, with empty adS space having a mass of $M = -1$, while regular initial data can form a black hole only if they have $M > 0$. Finally, black holes cannot form from regular initial data at all in 2+1-dimensional gravity without a negative cosmological constant. Hence the effect of the cosmological constant in critical collapse cannot be just perturbative.

Pretorius and Choptuik [9] fine-tuned four 1-parameter families of circularly symmetric initial data to the threshold of prompt collapse (before reflection from the outer boundary) and found universal continuous self-similarity (CSS), Ricci scaling and mass scaling. This was confirmed in [10].

Setting $\Lambda = 0$ as a heuristic starting point, Garfinkle [11] found a countable family of analytic CSS solutions and gave some numerical evidence that the $n = 4$ member of the family agrees with the near-critical evolutions of [9], at least inside the lightcone of the accumulation point. Garfinkle and Gundlach [13] showed that the Garfinkle solutions have $n - 1$ growing perturbation modes, thus apparently ruling out Garfinkle's $n = 4$ solution as the critical one. Cavaglià, Clément and Fabbri [16] showed that the Garfinkle solution(s) can be perturbatively corrected for $\Lambda < 0$, and that this does not change its perturbation spectrum. They also noted that when Λ is taken into account the lightcone of the $n = 4$ Garfinkle solution is no longer a marginally outer-trapped surface (MOTS) – something that would otherwise independently rule it out as a critical solution.

In the numerical part of our paper, we have repeated the time evolutions of [9], using essentially the same algorithm (coded independently), and re-analysed the data. In fine-tuned Gaussian data, we find a Ricci-scaling exponent of $\gamma \simeq 1.23(4)$, compatible with the $\gamma \simeq 1.2 \pm 0.05$ of [9], and a mass-scaling exponent of $\delta \simeq 0.68(4)$, roughly compatible with the value of $\delta \simeq 0.81$ given by [10]. (The value $\delta = 2\gamma$ of [9] is incorrect.)

We have also found excellent agreement between the $n = 4$ Choptuik solution and near-critical time evolutions inside the lightcone of the accumulation point. In particular, we can definitely rule out any other value of n. (Based on the fact that these have $n - 1$ growing modes, one might otherwise have suspected the $n = 2$ solution to be the critical one.) However, we can also definitely rule out the analytic continuation of the $n = 4$ Garfinkle solution beyond the lightcone as the critical solution there.

Rather, the observed critical solution outside the lightcone seems to be characterised by $M \simeq 0$, $\bar{r} \simeq (-\tilde{u})/2$, and $\phi \simeq c \ln(-\tilde{u}) + \text{const}$, where $\bar{r}$ is the area radius, $\tilde{u}$ retarded time normalised to proper time at the centre and with its origin suitably adjusted, and ϕ the scalar field.

In the theoretical part of our paper, we have shown that there is in fact a simple exact solution of this kind for $\Lambda = 0$, which can be matched to the Garfinkle solution at the lightcone. We call this the null-continued Garfinkle solution. We have also calculated the leading-order Λ correction of this solution and its perturbations. As the adjustment to $\Lambda < 0$ is done perturbatively in powers of Λ, the perturbation spectrum remains unchanged from the original Garfinkle solution. The Λ corrections remove the MOTS and thus one obstacle for this being the critical solution, but the obstacle of three growing modes remains, and the matching procedure has introduced a new obstacle, namely a lack of analyticity at the lightcone – our solution and its perturbations are only C^3 there. (All other known critical solutions are analytic at the lightcone, and are in fact defined by this property.)

Switching again to numerical time evolutions, we have taken this "amended Garfinkle solution" and taken five 1-parameter families of initial data through it, including the addition of its putative three growing modes. We do not find any evidence for three growing modes. Rather, our results are compatible with our theoretical predictions of $\gamma = 8/7$ and $\delta = 16/23$, based on a single growing mode with $k = 7/8$.

Based on the simple null continuation suggested by the numerics, we have also constructed an exact solution for $\Lambda < 0$ that gives the null-continuation and its first Λ correction when expanded to first order in Λ, and we expect that this holds to all orders. This is satisfactory from a theoretical point of view, but in our numerical evolutions we do not have enough numerical accuracy to see the difference between our exact outer solution and its approximation to first order in Λ, so we have used only the approximation in the main numerical part of this paper.

As discussed in Sec. III L above, the missing ingredient for constructing the exact critical solution is a way of analytically gluing together the Λ-corrected Garfinkle solution inside the lightcone to with new exact solution outside the lightcone. We conjecture that this analytic gluing procedure will somehow select $n = 4$ and remove two of the three growing modes.

[1] M. W. Choptuik Phys. Rev. Lett. **70**, 9, (1993).

[2] C. Gundlach and J. M. Martín-García, Living Rev. Relativity, **2007**-05 (2007).

[3] T. Koike, T. Hara and S. Adachi, Phys. Rev. Lett. **74**, 5170 (1995).

[4] P. Bizoń and A. Rostworowski, Phys. Rev. Lett. **107**, 031102 (2011).

[5] M. Birukou, V. Husain, G. Kunstatter, E. Vaz and M. Olivier, Phys. Rev. D **65**, 104036 (2002).

[6] J. Jałmużna, A. Rostworowski and P. Bizoń, Phys. Rev. D **84**, 085021 (2011).

[7] M. Maliborski and A. Rostworowski, Phys. Rev. Lett. **111**, 051102 (2013).

[8] P. Bizoń and J. Jałmużna, Phys. Rev. Lett. **111**, 041102 (2013).

[9] F. Pretorius, M. W. Choptuik, Phys. Rev. D **62**, 124012 (2000).

[10] V. Husain and M. Olivier, Class. Quant. Grav. **18**, L1 (2001).

[11] D. Garfinkle, Phys. Rev. D **63**, 044007 (2001).

[12] M. Reiterer and E. Trubowitz, Choptuik's critical spacetime exists, unpublished, arXiv:1203.3766.

[13] D. Garfinkle and C. Gundlach, Phys. Rev. D **66**, 044015 (2002).

[14] D. Christodoulou, Annals of Mathematics, **140**, 607 (1994).

[15] I. Hawke and J.M. Stewart, Class. Quantum Grav. **19**, 3687 (2002).

[16] M. Cavaglià, G. Clément and A. Fabbri, Phys. Rev. D **70**, 044010 (2004).

[17] Abramowitz and Stegun, Handbook of Mathematical Functions, accessed in an online version, `http://people.math.sfu.ca/~cbm/aands`, page 559.

[18] C. Gundlach and J. M. Martín-García, Phys. Rev. D **54**, 7353 (1996).